Journal of Marine Research, 68, 1–36, 2010

Journal of
MARINE RESEARCH

Volume 68, Number 1

Tides and Overtides in Long Island Sound

by Diane C. Bennett[1,2], James O'Donnell[1], W. Frank Bohlen[1] and Adam Houk[1]

ABSTRACT

Using observations obtained by acoustic Doppler profilers and coastal water level recorders, we describe the vertical and horizontal structure of the currents and sea level due to the principal tidal constituents in Long Island Sound, a shallow estuary in southern New England. As expected, the observations reveal that M_2 is the dominant constituent in both sea surface and velocity at all depths and sites. We also find evidence that the vertical structure of the M_2 tidal current ellipse parameters vary with the seasonal evolution of vertical stratification at some sites. By comparing our estimates of the vertical structure of the M_2 amplitudes to model predictions, we demonstrate that both uniform and vertically variable, time invariant eddy viscosities are not consistent with our measurements in the Sound. The current records from the western Sound contain significant overtides at the M_4 and M_6 frequencies with amplitudes and phases that are independent of depth. Though the M_4 amplitude decreases to the west in proportion to M_2, the M_6 amplifies. Since the dynamics that generate overtides also produce tidal residuals, this provides a sensitive diagnostic of the performances of numerical circulation models. We demonstrate that the observed along-Sound structure of the amplitude of the M_4 and M_6 overtides is only qualitatively consistent with the predictions of a nonlinear, laterally averaged layer model forced by a mean flow and sea level at the boundaries. Since neither the vertical structure of the principal tidal constituent nor the pattern of horizontal variation of the largest overtides can be explained using well established models, we conclude that they are fundamentally inadequate and should no longer be used for more than a basic qualitative understanding, and even then should be used with caution. We provide comprehensive tables of the tidal current parameters to facilitate the critical evaluation of future models of the circulation in the Sound.

1. Department of Marine Sciences, University of Connecticut, Groton, Connecticut, 06340, U.S.A.
2. Corresponding author. ***email: diane.bennett@uconn.edu***

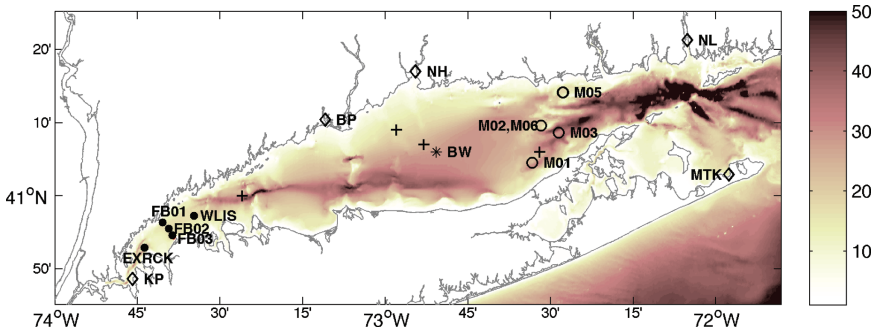

Figure 1. Bathymetric map of Long Island Sound. Diamonds show the location of NOAA tide gauges (KP = Kings Point, BP = Bridgeport, NH = New Haven, NL = New London, and MTK = Montauk), dots show LISICOS stations, asterisk shows central sound ADCP location, circles show LIS NSF stations, and pluses show historical current meter locations. Colors indicate depth in meters.

1. Introduction

Long Island Sound (LIS) is a shallow estuary located between Connecticut and Long Island, New York. Figure 1 shows the bathymetry and coastal geometry of the region. The circulation in the eastern end of LIS is forced by ocean tides through a deep and narrow channel known as The Race. The western end of the Sound is also connected to the ocean and the lower Hudson River Estuary through the East River, a dredged strait. The tidal circulation at the East River has been characterized by Bowman (1976), and Wilson *et al.* (1985) described the meteorologically forced motion. While the net volume exchanged at tidal frequencies is much smaller there than at the eastern boundary, Blumberg and Pritchard (1997) have shown that there is a strong mean westward volume flux of $310\,m^3\,s^{-1}$. This transport is the net result of a surface layer eastward flux of $260\,m^3\,s^{-1}$ and a lower layer westward flux of $570\,m^3\,s^{-1}$. The surface layer brings freshwater from the Hudson estuary into LIS causing the western Sound to be fresher than the eastern Sound, despite the fact that the major freshwater source, the Connecticut River, discharges into the Sound near the eastern boundary.

The high degree of urbanization and land development within the LIS watershed has significantly affected the Sound's ecosystem. Since at least the 1970s, the bottom waters of the western Sound have experienced hypoxia in the late summer as a consequence of nitrogen discharge from water treatment plants and agricultural practices (Parker and O'Reilly, 1991). In 1999 the lobster population in LIS experienced a catastrophic decline and investigation of the cause was hampered by the difficulty in simulating the transport of pollutants and the variability of stratification (Howell *et al.*, 2005). Well-calibrated circulation models are, therefore, critical to the wise development of management and remediation strategies.

The strongest tidal constituent in sea level variations in Long Island Sound is the semi-diurnal lunar, or M_2, signal (Swanson, 1976). The amplitude of the M_2 is smaller in the east

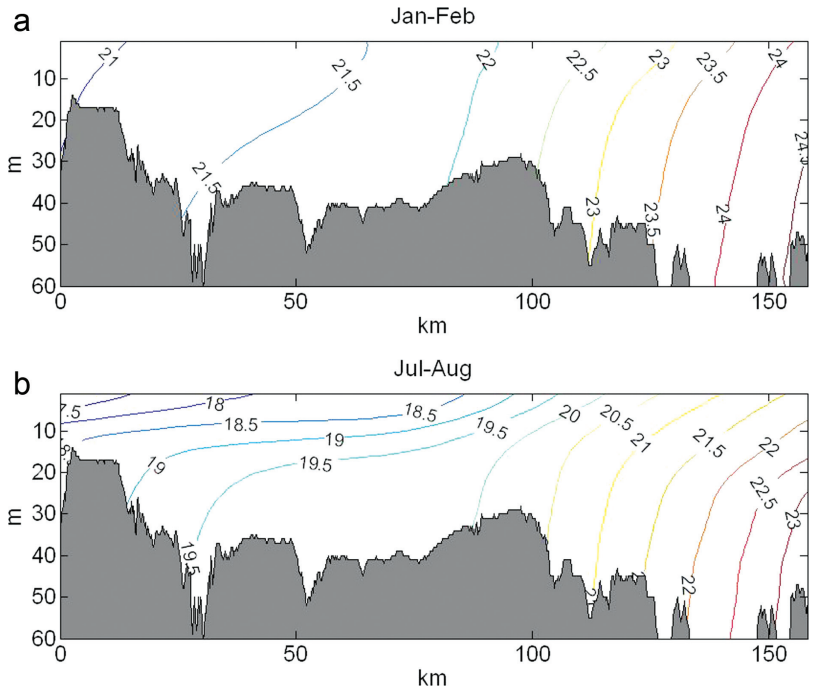

Figure 2. Density climatology along the central axis of Long Island Sound for winter (a) and summer (b).

and increases to the west. Wong (1991) observed that at the western end of the Sound the East River creates an imperfect reflecting wall at tidal frequencies, and the observed amplification is consistent with the fact that the length of the Sound is close to a quarter of the M_2 wavelength and is therefore near resonance. Few long-term current velocity measurements are available in LIS, but according to the vertically averaged model of Kenefick (1985) and the model and observations of Bogden and O'Donnell (1998), tidal currents generally decrease in amplitude from east to west and have weak lateral variation.

The large scale structure of the hydrography of LIS was first described by Riley (1956). Since 1988 a comprehensive monitoring program with cruises at monthly (or higher) frequency throughout the Sound has been undertaken by the Connecticut Department of Environmental Protection (CTDEP). Kaputa and Olsen (2000), Gay *et al.* (2004) and Lee and Lwiza (2005) provide a thorough analysis of this data set. Figure 2a shows the along-Sound structure of the density field in the winter computed by averaging all January and February observations at CTDEP stations along the central axis of LIS. The July-August distribution is shown in Figure 2b. The wintertime stratification in the western Sound associated with the distribution of freshwater is substantially augmented in the summer by the thermal stratification. It is therefore important to establish whether this changes the character of the tidal current structure.

The evaluation of circulation models for LIS has been hindered by a lack of observations with which to refine the simulations and evaluate the veracity of the predictions. Murphy (1980) and Kenefick (1985) developed similar two dimensional vertically averaged barotropic (2D) models of the area and showed that they could simulate the variation in the sea level observed by coastal tide gages. They also compared predicted vertically averaged current amplitude and phase to estimates obtained from short current meter deployments in the central Sound (see Gordon and Pilbeam (1975)).

Skill evaluation of the current estimates was limited because only measurements at a few near bottom and near surface locations were available. Since discrepancies between the model and observations could not be separated into measurement errors and real differences between the vertically averaged current and that at a fixed level, a critical assessment of the suitability of the model dynamics could not be completed. Bogden and O'Donnell (1998) combined moored, fixed level current meter observations with ship surveys using an acoustic Doppler current profiling system (ADCP) to estimate the relative magnitudes of the expected model-data differences for their implementation of the 2D model and demonstrated that the model and the mooring data were not inconsistent.

Since it is clear that the vertical structure of the circulation is critical to determining the transport and fate of material in estuaries, Blumberg and Galperin (1990), Schmalz (1993), Valle-Levinson and Wilson (1994), and Signell *et al.* (1998) developed three-dimensional circulation models for LIS. These models were evaluated using sea level observations and current measurements from a series of bottom mounted ADCP deployments conducted in 1988-89 by the National Oceanic and Atmospheric Administration (NOAA), which was summarized by Earwaker (1990). In this program instruments were cycled among the stations and long records were only obtained in the East River, the central Sound and the Race.

The seasonal variation in vertical stratification is the most extreme in the western Sound (see Fig. 2) and the horizontal gradients in dissolved oxygen are maximal there, and so the absence of current measurements in this region seriously limits the development and testing of transport models. In this paper we present a program designed to describe the structure of the tides in the western Sound and augment this data set with previously unpublished observations in the eastern and central Sound. We summarize all the observations that resolve the vertical structure of the tidal circulation in LIS and elucidate the spatial and temporal variability of the major constituents. We also provide tables that can be used to evaluate and compare transport models in the future.

This data set provides high resolution of both the vertical and horizontal variations of the amplitude and phase of the tidal currents in LIS and so we quantitatively assess whether the classic models of frictional barotropic dynamics are consistent with these observations. In particular, we assess whether simple vertical eddy viscosity models can describe the vertical structure of the main semidiurnal constituent (M_2), and whether a laterally averaged model with quadratic bottom friction and a realistic mean transport can describe the amplification of the M_2 and the associated generation of overtides. These models are often used to investigate

the dynamics of similar systems; recently, the assumption of time-invariant vertical eddy viscosity was used by Winant (2007) and Li *et al.* (1998), and Parker and O'Reilly's (1991) explanation of the generating mechanisms of tidal harmonics by nonlinear effects, on which our laterally averaged model is based, has been cited many times, by Hench and Luettich (2003), Andersen *et al.* (2006), Valle-Levinson *et al.* (2007), and Breaker *et al.* (2008), among others. Until now it has not been possible to demonstrate that they are based on invalid assumptions. Therefore, we make use of our extensive data set, which spans a wide range of stratification conditions, to assess rigorously the accuracy of these models in an estuarine setting. We also examine how tidal ellipses in LIS are affected by seasonal changes in stratification in order to assess whether the effects observed in strongly stratified conditions by Visser *et al.* (1994), Souza and Simpson (1996) and Codiga and Rear (2004) also apply in a more weakly stratified estuary.

In the next section we describe the data sources used and in Section 3 we summarize the models we evaluate. We summarize the distribution of the tidal constituents in Section 4 and then compare the predictions of the models to the observations. Section 5 contains a discussion of the results and in Section 6 we provide a summary of our conclusions.

2. Observations

A series of ADCPs were deployed on bottom frames in western LIS as a component of the Long Island Sound Integrated Coastal Observing System (LISICOS). The deployment locations are shown in Figure 1, labeled EXRCK, FB01, FB02, FB03, and WLIS. The ADCPs were generally co-located with buoys that measured conductivity, temperature, pressure, and dissolved oxygen at three levels (near surface, mid-depth and near-bottom) to observe the variability in stratification. These observations are described in O'Donnell *et al.* (2008). Table 1 lists the locations of all the current velocity measurements used in this analysis together with the mean water depth, deployment times and the ADCP sampling parameters. During the summer 2005 deployment only, station FB03 was located closer to the coast than its location in Figure 1.

Five records from 300 kHz broadband ADCPs deployed on the bottom in eastern LIS in 1998 at the locations labeled M01-3 and M05-6 in Figure 1 were available from an earlier study, two of which were co-located. Data from a similar 600 kHz ADCP deployment in central LIS were utilized as well. This deployment extended for more than a year, from 2005 to 2006, with four short interruptions. The deployment details of these instruments are also listed in Table 1.

Finally, several historical observations of current velocities that included harmonic analysis of the M_2 component in Long Island Sound were also utilized for model comparisons. These are derived from Gordon and Pilbeam (1975) and from Cobb *et al.* (1978). The locations of these observations are indicated in Figure 1 by + symbols.

Records of sea surface height are available at several locations in Long Island Sound from NOAA's web site (http://tidesonline.nos.noaa.gov). We employ data from stations at

Table 1. Details of ADCP frame deployments. Note that ppe stands for 'pings per ensemble'.

Deployment Dates	Station	Latitude (°N)	Longitude (°W)	Frequ. (kHz)	Mode	ppe	Bin size (m)	Min rng (m)	Depth (m)
Feb. 16 - May 13, 2005	WLIS	40° 57.290'	73° 34.834'	600	1	100	0.5	1.73	19.15
July 12 - Sept. 29, 2005	EXRCK	40° 52.944'	73° 43.724'	600	12	60	0.1	1.26	20.61
	FB01	40° 56.568'	73° 40.675'	300	1	300	1	3.11	12.67
	FB02	40° 55.405'	73° 39.509'	300	1	300	1	3.11	17.23
	FB03	40° 54.220'	73° 38.417'	600	1	300	1	2.71	13.23
June 30 - Aug. 16, 2006	EXRCK	40° 52.945'	73° 43.721'	600	12	120	0.5	1.61	20.43
	FB01	40° 56.359'	73° 40.450'	300	1	120	1	3.24	13.48
	FB02	40° 55.518'	73° 39.392'	600	12	120	0.5	1.61	17.61
	FB03	40° 54.600'	73° 38.722'	300	1	120	1	3.24	16.22
	WLIS	40° 57.298'	73° 34.740'	300	12	120	1	3.22	19.46
September 11, 2006 -	EXRCK	40° 52.949'	73° 43.737'	600	12	60	0.5	1.61	19.83
May 14, 2007	FB01	40° 56.363'	73° 40.453'	300	1	120	1	3.21	13.46
	FB02	40° 55.516'	73° 39.392'	600	12	60	0.5	1.61	17.62
	FB03	40° 54.600'	73° 38.722'	300	1	120	1	3.22	16.02
	WLIS	40° 57.247'	73° 34.742'	300	12	60	1	3.22	19.51
July 18 -	EXRCK	40° 52.949'	73° 43.737'	600	12	60	0.5	1.62	21.80
November 28, 2007	FB01	40° 56.363'	73° 40.453'	300	1	120	1	3.22	13.51
	FB02	40° 55.516'	73° 39.392'	600	12	120	0.5	1.61	17.63
	FB03	40° 54.600'	73° 38.722'	300	1	120	1	3.23	16.14
	WLIS	40° 57.247'	73° 34.742'	300	12	60	1	3.24	19.15
July 24 - Oct. 15, 1997	M01	41° 4.54'	72° 33.36'	300	1	50	0.5	3.15	20.9
July 24 - Oct. 15, 1997	M02	41° 9.60'	72° 31.74'	300	1	50	0.5	3.15	20.7
July 24 - Oct. 8, 1997	M03	41° 8.65'	72° 28.54'	300	1	50	0.5	3.15	33.2
July 24 - Oct. 15, 1997	M04	41° 14.17'	72° 27.77'	300	1	50	0.5	3.15	19.0
Oct. 16 - Dec. 4, 1997	M05	41° 14.15'	72° 27.72'	300	1	50	0.5	3.15	18.7
Oct. 16 - Dec. 4, 1997	M06	41° 9.60'	72° 31.71'	300	1	50	0.5	3.15	20.6
Sept. 27 2005 - Oct. 17 2006	BW	41° 6.00'	72° 50.73'	600	1	50	0.5	1.62	28.7

Kings Point, NY, Bridgeport, CT, New Haven, CT, New London, CT, and Montauk, NY, which are indicated by diamonds on the map in Figure 1. Measurements from the Battery in the East River were also used to help understand the tidal dynamics.

3. Theory and analysis

a. Vertical structure

Simple models that are tractable using analytic approaches have proven extremely valuable in oceanography. Ianniello (1977a, b) demonstrated this in an early model of the vertical structure of tides in an estuary. He argued that the effects of advection of momentum and the baroclinic pressure gradient were small compared to the local acceleration and the barotropic pressure gradient and that the vertical gradient of the turbulent eddy stress was important throughout the water column. He then approximated the along-estuary momentum balance by

$$\frac{\partial u}{\partial t} = -g\frac{\partial \eta}{\partial x} + \frac{\partial}{\partial z}\left(A_z \frac{\partial u}{\partial z}\right) \tag{1}$$

where u is the along-channel velocity in the x direction, z is the vertical coordinate, t is time, g is the vertical acceleration due to gravity, $z = \eta$ is the sea surface level, and A_z is the vertical eddy viscosity. This model assumes that the Reynolds stresses can be approximated by an eddy viscosity coefficient following Proudman (1953).

Ianniello also formulated a linearized continuity equation that allowed along-estuary variations in bottom depth and channel width. He sought periodic solutions for the structure of the laterally averaged velocity and sea level in a semi-enclosed channel of length L forced by a single frequency, ω, with amplitude η_0 at the ocean boundary ($x = 0$). He did not ignore the Coriolis acceleration but argued that in a channel with a large length-to-width ratio, the contribution of the lateral velocity to the along-channel momentum budget would be small. More recently, Winant (2007) noted that even though vertically integrated transports are only weakly influenced by rotation, the velocity structure can still be significantly affected. He generalized Ianniello's model to include the Coriolis effect and his modified along-estuary momentum equation is

$$\frac{\partial u}{\partial t} - fv = -g\frac{\partial \eta}{\partial x} + A_z \frac{\partial^2 u}{\partial z^2}. \tag{2}$$

In this equation, f is the Coriolis parameter and v is the across-channel (y direction) velocity component. Note that the Winant solution uses a constant eddy viscosity. While this across-estuary momentum equation is only slightly modified from Ianiello's solution, Winant also included the across-estuary momentum equation,

$$\frac{\partial v}{\partial t} + fu = -g\frac{\partial \eta}{\partial y} + A_z \frac{\partial^2 v}{\partial z^2}. \tag{3}$$

Winant showed that for weak to moderate friction, rotation can drive lateral flows that are of similar magnitude to the along-axis flow, and therefore cross-estuary tidal flows may be important in systems where rotation plays a role.

Ianniello showed that the velocity field can be written in the separable form $u(x, z, t) = U(z)a(x)\exp(i\omega t)$ where $i = \sqrt{-1}$. Here, $a(x)$ and $U(z)$ are complex functions. $a(x)$ describes the along-channel variation in the amplitude and phase, and $U(z)$ describes the vertical structure of the velocity. The tidal velocity amplitude as a function of depth has a simple analytic solution when A_z is constant. The velocity solution is controlled by the dimensionless variable d_0, the ratio of the actual depth to the frictional depth. As d_0 increases, friction affects a smaller percentage of the water column.

Prandtl (1925) proposed the mixing length hypothesis for the effect of turbulence in a flow that varies in one dimension and estimated that

$$A_z = l_m^2 \left| \frac{dU}{dz} \right| \tag{4}$$

where the mixing length (l_m) was prescribed empirically. The structure of an open channel flow with a free surface at $z = 0$ and a rigid boundary at $z = -h$ was found to be consistent with $l_m = \kappa(z + h)$ where $\kappa \approx 0.4$ is known as the von Karman constant. Subsequently, there has been considerable literature on the parameterizations of l_m and A_z (e.g., see Mellor and Yamada, 1974). Ianniello considered several cases of an algebraic length scale closure in which A_z increases with distance from the bed. He showed that the vertical structure of tidal flow was only sensitive to the parameterization of $A_z(z)$ near the bed where vertical shear is large, and that $d_0 \approx 2$ was consistent with the observations of the vertical structure of tidal flows available to him. This has been confirmed by similar models (e.g. Prandle, 1982).

Using numerical integration to retain flexibility in the form of A_z, we solved for u in Eq. (1) by reducing it to a split boundary value problem in two simultaneous first order equations. While it is possible to use this technique to test cases where there is no analytic solution for a particular eddy viscosity profile, we will be discussing the eddy viscosity cases examined by Ianniello, which do have analytic solutions, in order to re-evaluate these basic scenarios using our tidal velocity amplitude data. We also solved for u in Eq. (2) and v in Eq. (3) in a similar fashion while retaining a constant form for A_z to evaluate the modified model of Winant (2007).

Adding rotation to the one-dimensional vertical model for tidal flow allows a more rigorous verification of the analytic model; however, we were interested in further quantifying the effects that rotation has on both the flow and rotational characteristics of the tidal ellipse. The effects of stratification on the vertical profile of the semidiurnal tidal current ellipse have been described for a region of freshwater influence in the North Sea by Souza and Simpson (1996) and Visser *et al.* (1994). It was observed that during periods in which the water was relatively well mixed, surface ellipses were nearly degenerate and had a small

cyclonic component near the seabed. During times when the water was stratified, an anticyclonic rotation was observed at the surface and the cyclonic rotation near the seabed was enhanced. A change in orientation was also noted during times of higher stratification.

Souza and Simpson (1996) proposed that the change in the rotary motion of the tides was a consequence of the independent frictional layer depths of the cyclonic (δ_+) and anticyclonic (δ_-) rotating tidal components. Following Prandle (1982), the bottom layer frictional depths can be written as

$$\delta_+ = \left(\frac{2A_z}{\omega + f}\right)^{1/2}, \quad \delta_- = \left(\frac{2A_z}{\omega - f}\right)^{1/2} \tag{5}$$

where A_z and ω are the turbulent eddy viscosity and tidal frequency, as before, and f is the Coriolis parameter.

Eq. 5 implies that the cyclonic component has a smaller frictional depth than the anticyclonic component. Souza and Simpson (1996) argued that if the ellipse is degenerate at the surface (rectilinear flow) where the cyclonic and anticyclonic components are equal, then the cyclonic component will remain constant with depth until its frictional layer is reached near bottom, while the anticyclonic component will begin to decay higher in the water column as a result of its larger frictional depth. This will lead to a near bottom ellipse with cyclonic rotation. Assuming that the barotropic pressure gradient remains unchanged, stratification should reduce the eddy viscosity in the pycnocline which, they proposed, would have no substantial influence on the cyclonic component if the pycnocline was already above δ_+, its boundary layer thickness. However, the reduced effect of bottom friction on the anticyclonic component would allow it to have greater amplitude at the surface, and would reduce it further in the bottom layer. This argument suggests that during stratified periods the surface waters would exhibit an anticyclonic rotation of the semidiurnal current ellipse and a cyclonic rotation near bottom, a prediction found to be consistent with the observations of Souza and Simpson (1996). By similarly separating our data into periods of higher and lower stratification, we were able to analyze whether stratification in Long Island Sound produced the same effects.

b. Along-Sound structure

Parker (1984) presented a very thorough analysis of a one dimensional vertically- and laterally- averaged model of tides in estuaries and qualitatively described how the nonlinearities in the momentum and mass balances lead to the generation of overtides. However, the absence of current observations means that this theory has yet to be quantitatively evaluated. The along-Sound resolution of the data available in Long Island Sound allows for the evaluation of this simple model by comparing the observed and predicted amplification of the principal tidal constituent and the distribution of the mean transport on overtides.

Parker addresses two mechanisms that affect the generation of higher harmonics: the interaction of several major constituents, and the presence of mean flow. The former was

recently examined by Dworak and Gomez-Valdes (2005) in an estuary where both diurnal and semidiurnal astronomical forcing were strong. We will use similar techniques to evaluate the effects of river flow on overtides, the second mechanism.

In the model of Parker (1984) the cross-sectionally averaged along-channel velocity is written as $\bar{u}$ and the estuarine geometry is assumed to be rectangular. The along channel momentum equation (including the advection of momentum term) is then integrated from the bottom ($z = -h$) to the surface ($z = \eta$) and across-channel (of width b) to yield

$$\frac{\partial \bar{u}}{\partial t} + \bar{u}\frac{\partial \bar{u}}{\partial x} = -g\frac{\partial \eta}{\partial x} - C_D\frac{1}{h+\eta}\bar{u}|\bar{u}| \tag{6}$$

and the continuity equation can be similarly expressed as

$$\frac{\partial \eta}{\partial t} + \frac{1}{b}\frac{\partial}{\partial x}(b(h+\eta)\bar{u}) = 0 \tag{7}$$

with imposed boundary conditions of zero surface stress and bottom stress $\tau(-h) = \rho C_D \bar{u}|\bar{u}|$, where C_D is the bottom drag coefficient. The text of Dean and Dalrymple (1991) (see Chapter 5) develops this formulation in detail. Note that this form neglects the effect of horizontal variations in the vertical structure of the horizontal velocity.

This system contains four nonlinear effects: in the momentum equation, the advection of momentum ($\bar{u}\frac{\partial \bar{u}}{\partial x}$), quadratic friction ($\bar{u}|\bar{u}|$), and the asymmetry of the friction term at high and low water ($\bar{u}|\bar{u}|\eta^{-1}$), and the Stokes flux ($\eta\bar{u}$) in the continuity equation. A substantial simplification can be achieved by assuming that ϵ, the ratio of the sea surface fluctuations to the mean water depth, is less than one and then writing the dependent variables as a power series ($\eta = \eta_0 + \epsilon\eta_1 + \epsilon^2\eta_2 + \ldots$ and $\bar{u} = \bar{u_0} + \epsilon\bar{u_1} + \epsilon^2\bar{u_2} + \ldots$). This leads to an infinite series of linear equations that can be solved sequentially. The frictional term can be simplified with a Fourier expansion of $\bar{u}|\bar{u}|$ as shown by Proudman (1953). When zero mean periodic forcing of the sea level is enforced as a boundary condition for $\eta_0(x = 0)$ then, for simple forms of $h(x)$ and $b(x)$, the lowest order equations have a harmonic solution at the imposed frequency since they are linear in the dependent variables. Note that Inoue and Garrett (2007) have recently generalized this approach to two dimensional flows.

The second order equations are also linear in η_1 and $\bar{u}_1$; however, they are "forced" by inhomogeneous terms containing products of η_0 and $\bar{u}_0$ that arise from the expansion of the nonlinearities discussed above. Parker (1984) provides a clear explanation of the physical mechanisms that lead to the generation of harmonics. The details of this approach can be found in, for example, Li and O'Donnell (1997; 2005). Here it is sufficient to appreciate that the $\bar{u}\frac{\partial \bar{u}}{\partial x}$ and $\eta\bar{u}$ terms lead to a steady (zero frequency) forcing of η_1 and $\bar{u}_1$ and oscillatory forcing at even harmonics of the frequency imposed at the boundary. If, as is the case in LIS, the ocean tide causes fluctuations at the ocean boundary at the M_2 frequency, then the second order solutions would contain a mean component and the $M_{4,8,12,\ldots}$ constituents. In contrast, the terms proportional to $\bar{u}|\bar{u}|$ lead to a mean flow and odd harmonics in the second

order solution. For M_2 ocean forcing, we would then expect to observe $M_{6,10,\ldots}$ constituents in the basin as well.

When there is a mean flow imposed in an estuary by a river or by a mean pressure gradient across the boundaries of the basin in addition to an oscillatory tidal constituent, then the $\bar{u}|\bar{u}|$ term also generates even harmonics and the forcing of the odd harmonics is reduced. Parker (1984) shows that for an estuary with constant width and depth, when the amplitude of the principal tidal current constituent is much larger than the magnitude of the mean current, the dependence of odd harmonic forcing magnitude on the mean flow is small but the effect on even harmonics increases rapidly with the mean flow.

Blumberg and Pritchard (1997) present strong evidence of a mean transport through LIS and conservation of mass suggests that the mean velocity must increase westward as the cross-sectional area of the Sound is reduced. The analysis of the effects of the nonlinear interactions then suggest the qualitative prediction that the M_4 and M_6 tidal current constituents, and perhaps higher harmonics, should be more energetic in the western Sound than in the east. Further, if there is seasonal variation in the magnitude of the mean flow, the M_4 amplitudes may reflect that variability.

Since the geometry of LIS is quite complicated, we obtain numerical solutions to the momentum and continuity equations following the method described by Parker (1984). We use this model to evaluate whether the observed overtide amplitude and phase distribution can be explained by the long wave equations in order to establish whether a more sophisticated model is essential.

4. Results

To characterize the tidal variation of sea level in the Sound and to inform model developers, we present in Table 2 estimates of the amplitude and phase, together with their uncertainties, of the five largest tidal constituents of sea level observed at Kings Point, Bridgeport, New Haven, New London, and Montauk, using the hourly records made available by NOAA for the period of 1 January to 31 December, 2005 and t-tide (Pawlowicz *et al.*, 2002), an efficient and well-tested implementation of harmonic analysis in MATLAB. Comparison of the results of our analysis to those of NOAA, available at http://co-ops.nos.noaa.gov, demonstrates that at all stations the M_2 amplitudes agree to within 2 cm and the phases differ by less than a degree. There is no evidence of systematic biases in our estimates. We also find that the amplitudes of the less energetic constituents are consistent with those of NOAA. We present the results here both for validation of technique and to provide both sea level and velocity data for LIS in one location.

Throughout the Sound, the M_2 constituent dominates the sea level variability. At Montauk the N_2 and K_1 are of equal amplitude and approximately 25 percent of the M_2; the S_2 and O_1 are slightly smaller. The semidiurnal constituents amplify to the west, and at New Haven and Bridgeport the M_2, N_2 and S_2, the three highest amplitude signals in the sea level records, are all a factor of three larger than at Montauk. Analysis of the Kings Point record, at the

Table 2. Amplitudes and phases of five largest constituents at NOAA stations in Long Island Sound. Phases are relative to Greenwich, and smaller values indicate a phase advance.

Constituent		Amplitude (m)	Phase (degrees)
Kings Point, NY:	M_2	1.1608 ± 0.007	115.84 ± 0.3
	N_2	0.2285 ± 0.006	94.83 ± 1.6
	S_2	0.1922 ± 0.006	142.73 ± 2.0
	K_1	0.1033 ± 0.007	192.68 ± 3.5
	M_6	0.0849 ± 0.006	162.01 ± 3.9
Bridgeport, CT:	M_2	0.9959 ± 0.005	109.57 ± 0.3
	N_2	0.1954 ± 0.006	88.39 ± 1.8
	S_2	0.1577 ± 0.005	136.09 ± 1.9
	K_1	0.0973 ± 0.006	190.81 ± 3.4
	O_1	0.0589 ± 0.006	219.21 ± 5.3
New Haven, CT:	M_2	0.9025 ± 0.004	106.16 ± 0.3
	N_2	0.1759 ± 0.004	84.86 ± 1.1
	S_2	0.1417 ± 0.004	132.11 ± 1.5
	K_1	0.0942 ± 0.005	188.63 ± 3.6
	O_1	0.0552 ± 0.005	219.28 ± 5.8
New London, CT:	M_2	0.3615 ± 0.002	59.53 ± 0.3
	N_2	0.0812 ± 0.002	35.74 ± 1.6
	K_1	0.0721 ± 0.005	178.56 ± 3.6
	S_2	0.0640 ± 0.002	71.7 ± 2.1
	O_1	0.0456 ± 0.004	211.09 ± 5.4
Montauk, NY:	M_2	0.2832 ± 0.006	47.42 ± 1.5
	N_2	0.0712 ± 0.006	27.24 ± 5.8
	K_1	0.0708 ± 0.008	173.14 ± 6.8
	S_2	0.0594 ± 0.006	60.56 ± 6.9
	O_1	0.0465 ± 0.007	213.75 ± 9.0

western end of the Sound, shows that the semidiurnal constituents continue to amplify to the west. At this location the four largest constituents are the same as at the stations to the east, but the M_6 replaces the O_1 as the fifth in rank.

The NOAA tidal stations are all located at the coast, and so we also performed a harmonic analysis of the sea surface level time series at the mid-Sound ADCP frames, which we obtained from the instruments' acoustic backscatter data. The amplitude and phase of the five largest constituents at each station are presented in Table 3. Note that the duration of these deployments was significantly shorter than the year-long sea level records (see Table 1); this results in a three fold increase in the uncertainty of the amplitude and phase estimates. Nonetheless, the five western Sound stations agree well with the coastal stations, with the amplitudes and phases of the dominant constituents (M_2, N_2, S_2, K_1 and O_1) lying between the values at Bridgeport and Kings Point. There is no evidence from our observations that the tidal response at the coastal stations are substantially influenced by the local topography and geometry.

The main characteristics of our analysis of the velocity records are summarized in Tables 4 and 5, which contain the tidal ellipse parameters at near surface and near bottom levels for

Table 3. Amplitudes and phases of five largest constituents at LISICOS stations in Long Island Sound. Phases are relative to the predicted maximum equilibrium tide at Greenwich, and smaller values indicate a phase advance.

Constituent		Amplitude (m)	Phase (degrees)
EXRCK:	M_2	1.1128 ± 0.031	114.51 ± 1.9
	N_2	0.2281 ± 0.034	94.99 ± 8.7
	S_2	0.1971 ± 0.033	146.63 ± 10
	K_1	0.1381 ± 0.034	194.00 ± 15
	O_1	0.0759 ± 0.033	226.84 ± 26
FB01:	M_2	1.1151 ± 0.022	113.69 ± 1.1
	N_2	0.2294 ± 0.023	93.39 ± 5.4
	S_2	0.2022 ± 0.021	149.15 ± 6.4
	K_1	0.1571 ± 0.029	190.90 ± 10
	O_1	0.0749 ± 0.030	221.79 ± 23
FB02:	M_2	1.1116 ± 0.026	113.58 ± 1.2
	N_2	0.2261 ± 0.024	92.34 ± 6.3
	S_2	0.1859 ± 0.025	149.44 ± 7.7
	K_1	0.1327 ± 0.030	193.18 ± 12
	O_1	0.0686 ± 0.027	225.04 ± 25
FB03:	M_2	1.1113 ± 0.023	113.59 ± 1.2
	N_2	0.2256 ± 0.021	92.97 ± 5.7
	S_2	0.1884 ± 0.022	147.37 ± 7.3
	K_1	0.1303 ± 0.033	184.17 ± 13
	O_1	0.0686 ± 0.033	226.83 ± 31
WLIS:	M_2	1.0847 ± 0.028	112.84 ± 1.4
	N_2	0.2055 ± 0.030	91.71 ± 7.8
	S_2	0.1945 ± 0.028	145.73 ± 8.8
	K_1	0.1158 ± 0.031	182.34 ± 19
	O_1	0.0706 ± 0.032	217.32 ± 28

the five strongest constituents at the eastern and western Sound stations, respectively. We employ the convention used by Pawlowicz *et al.* (2002) and represent the tidal current ellipse in the hodograph plane for a constituent in terms of the semi-major and semi-minor axes, the orientation in degrees north of east, and the phase delay relative to the maximum equilibrium forcing at Greenwich.

These tables confirm that the largest amplitude tidal current constituent at all sites is at the M_2 frequency, which is consistent with the sea surface amplitude results. Near surface velocity amplitudes at the western Sound stations range from 18 to 28 cm s^{-1}. In the eastern Sound amplitudes are much larger, approaching 1 m s^{-1} near the surface at station M03. At all sampling stations the M_2 velocities show a substantial decrease with depth. Near the surface in the eastern Sound, N_2 and S_2 are the second and third largest amplitude constituents and are approximately 25 percent of the M_2 amplitude. The fourth and fifth largest species are not consistent across the four stations; however, the three constituents present are L_2, K_1 and M_4 in varying orders of importance, with amplitudes approximately

Table 4. Tidal velocity ellipse properties of the five largest constituents of the near surface and near bottom in the eastern Sound. A negative semi-minor axis amplitude indicates rotation in the clockwise direction. Phases are Greenwich phases, and a smaller phase indicates an advance. Orientations are counterclockwise from due east.

		Near surface					Near bottom			
		maj amp ($cm\,s^{-1}$)	Min amp ($cm\,s^{-1}$)	Phase (deg)	Orientation (deg)		maj amp ($cm\,s^{-1}$)	Min amp ($cm\,s^{-1}$)	Phase (deg)	Orientation (deg)
BW	M2	37 ± 1	-2.5 ± 0.7	242 ± 1	182 ± 1	M2	28 ± 0.5	4.8 ± 0.4	221 ± 1	172 ± 1
	N2	8 ± 1	-0.6 ± 0.7	223 ± 5	182 ± 6	N2	6 ± 0.5	0.8 ± 0.4	200 ± 5	170 ± 4
	S2	6 ± 1	-0.4 ± 0.7	266 ± 6	185 ± 7	S2	5 ± 0.4	0.8 ± 0.4	247 ± 6	176 ± 5
	L2	2 ± 1	-0.3 ± 0.8	276 ± 28	186 ± 29	L2	2 ± 0.5	-0.2 ± 0.5	265 ± 17	162 ± 14
	MSF	2 ± 1	-0.6 ± 1.3	231 ± 62	220 ± 47	K1	1 ± 0.2	0.1 ± 0.2	225 ± 13	75 ± 11
M01	M2	65 ± 2	-7.3 ± 1.5	231 ± 2	34 ± 2	M2	43 ± 1.2	11.9 ± 1.2	218 ± 2	29 ± 2
	N2	12 ± 2	-0.8 ± 1.9	221 ± 8	41 ± 8	N2	10 ± 1.2	1.7 ± 1.2	211 ± 7	24 ± 8
	S2	12 ± 2	-1.1 ± 1.6	234 ± 8	33 ± 9	S2	7 ± 1.1	1.5 ± 1.2	228 ± 10	36 ± 9
	K1	5 ± 1	-0.6 ± 1.1	292 ± 14	15 ± 13	L2	4 ± 1.4	1.0 ± 1.3	181 ± 23	159 ± 22
	L2	4 ± 1	-3.4 ± 1.6	284 ± 70	24 ± 65	K1	2 ± 0.5	0.1 ± 0.4	317 ± 11	56 ± 12
M02	M2	74 ± 2	-9.2 ± 0.8	229 ± 1	1 ± 1	M2	52 ± 0.8	-1.1 ± 0.5	217 ± 1	5 ± 1
	N2	16 ± 1	-1.0 ± 0.8	218 ± 5	3 ± 3	N2	13 ± 0.9	-0.9 ± 0.5	211 ± 4	3 ± 2
	S2	12 ± 2	-0.9 ± 0.8	226 ± 8	179 ± 4	S2	9 ± 0.8	-0.5 ± 0.6	223 ± 5	5 ± 4
	L2	5 ± 2	-1.9 ± 0.9	262 ± 22	179 ± 14	L2	3 ± 0.9	0.2 ± 0.6	213 ± 15	7 ± 10
	M4	5 ± 1	-0.9 ± 0.4	264 ± 9	174 ± 7	M6	3 ± 0.6	0.6 ± 0.3	290 ± 13	173 ± 7
M06	M2	70 ± 2	-7.4 ± 0.6	227 ± 1	2 ± 1	M2	54 ± 1.1	-4.0 ± 0.6	222 ± 1	5 ± 1
	N2	13 ± 2	-1.0 ± 0.7	370 ± 7	3 ± 3	N2	11 ± 1.1	-1.2 ± 0.6	366 ± 6	5 ± 3
	S2	12 ± 2	-0.3 ± 0.6	239 ± 9	5 ± 3	S2	10 ± 1.3	-0.5 ± 0.6	233 ± 7	2 ± 4
	K1	4 ± 1	-0.1 ± 0.8	284 ± 16	2 ± 10	K1	3 ± 1.0	-0.2 ± 0.4	286 ± 14	178 ± 6
	L2	4 ± 2	-1.5 ± 0.8	273 ± 35	12 ± 17	M4	3 ± 0.5	-0.1 ± 0.5	273 ± 10	150 ± 9
M03	M2	90 ± 2	-18.7 ± 1.9	234 ± 1	22 ± 1	M2	50 ± 0.8	11.3 ± 0.7	230 ± 1	25 ± 1
	N2	19 ± 2	-2.1 ± 1.8	226 ± 6	19 ± 6	N2	13 ± 0.7	2.1 ± 0.9	222 ± 3	25 ± 3
	S2	14 ± 2	-1.6 ± 1.9	237 ± 8	19 ± 7	S2	10 ± 0.7	0.7 ± 0.8	236 ± 4	26 ± 5
	L2	8 ± 2	-4.8 ± 2.0	248 ± 29	34 ± 30	M4	3 ± 0.5	0.2 ± 0.4	229 ± 9	102 ± 6
	M4	6 ± 1	-3.4 ± 1.0	216 ± 21	129 ± 21	K1	3 ± 0.5	-0.1 ± 0.5	292 ± 10	35 ± 9
M05	M2	69 ± 2	-2.8 ± 1.3	211 ± 2	177 ± 1	M2	51 ± 1.0	-3.6 ± 0.9	207 ± 1	3 ± 1
	N2	13 ± 2	-0.4 ± 1.3	353 ± 9	176 ± 6	N2	10 ± 1.1	-1.1 ± 1.1	350 ± 7	2 ± 6
	S2	11 ± 2	0.8 ± 1.3	223 ± 12	3 ± 7	S2	9 ± 1.1	-1.3 ± 0.9	225 ± 8	173 ± 7
	L2	5 ± 2	-2.7 ± 1.8	270 ± 52	175 ± 40	M4	5 ± 0.6	2.7 ± 0.7	236 ± 17	19 ± 18
	K1	4 ± 1	0.6 ± 0.7	273 ± 17	179 ± 10	L2	4 ± 1.3	1.5 ± 1.3	248 ± 25	5 ± 25

Table 5. Tidal velocity ellipse properties of the five largest constituents of the near surface and near bottom in the western Sound. A negative semi-minor axis amplitude indicates rotation in the clockwise direction. Phases are Greenwich phases, and a smaller phase indicates an advance. Orientations are counterclockwise from due east.

		Near surface					Near bottom			
		maj amp ($cm\,s^{-1}$)	Min amp ($cm\,s^{-1}$)	Phase (deg)	Orientation (deg)		maj amp ($cm\,s^{-1}$)	Min amp ($cm\,s^{-1}$)	Phase (deg)	Orientation (deg)
EXRCK	M2	18 ± 0.4	0.1 ± 0.4	245 ± 1	40 ± 1	M2	13 ± 0.3	4.0 ± 0.3	230 ± 1	56 ± 1
	M6	5 ± 0.2	-0.3 ± 0.3	243 ± 3	40 ± 3	M6	4 ± 0.2	1.1 ± 0.2	233 ± 3	44 ± 3
	N2	4 ± 0.4	0.1 ± 0.4	209 ± 5	45 ± 5	2MN6	3 ± 0.2	0.6 ± 0.2	207 ± 5	44 ± 5
	2MN6	3 ± 0.2	-0.3 ± 0.3	217 ± 5	42 ± 5	N2	3 ± 0.3	0.8 ± 0.2	193 ± 7	42 ± 6
	M4	3 ± 0.2	-0.6 ± 0.2	271 ± 5	30 ± 5	S2	2 ± 0.2	0.2 ± 0.2	250 ± 8	41 ± 9
FB01	M2	24 ± 0.3	-0.5 ± 0.3	231 ± 1	42 ± 1	M2	21 ± 0.3	2.3 ± 0.3	224 ± 1	44 ± 1
	N2	5 ± 0.3	0.1 ± 0.3	201 ± 4	42 ± 4	M6	5 ± 0.2	0.1 ± 0.2	240 ± 3	41 ± 3
	M6	5 ± 0.2	0.0 ± 0.2	249 ± 3	42 ± 2	N2	4 ± 0.3	0.4 ± 0.3	199 ± 4	47 ± 4
	S2	4 ± 0.3	-0.1 ± 0.3	257 ± 5	44 ± 4	S2	4 ± 0.3	0.2 ± 0.2	250 ± 4	47 ± 4
	2MN6	3 ± 0.2	0.0 ± 0.2	225 ± 4	43 ± 4	2MN6	3 ± 0.2	0.1 ± 0.2	216 ± 4	43 ± 4
FB02	M2	24 ± 0.4	-2.2 ± 0.4	235 ± 1	39 ± 1	M2	17 ± 0.3	6.4 ± 0.3	213 ± 2	32 ± 2
	N2	5 ± 0.4	-0.2 ± 0.4	211 ± 5	40 ± 5	M6	4 ± 0.2	0.1 ± 0.2	237 ± 2	37 ± 2
	M6	4 ± 0.2	0.2 ± 0.2	251 ± 3	36 ± 3	N2	3 ± 0.3	1.2 ± 0.3	193 ± 7	39 ± 6
	S2	4 ± 0.4	0.1 ± 0.4	260 ± 7	34 ± 7	S2	3 ± 0.3	0.9 ± 0.3	247 ± 7	42 ± 7
	2MN6	3 ± 0.2	0.2 ± 0.2	225 ± 4	36 ± 5	2MN6	3 ± 0.2	0.2 ± 0.2	211 ± 4	37 ± 4
FB03a	M2	20 ± 0.5	-5.6 ± 0.5	193 ± 2	48 ± 2	M2	16 ± 0.4	-3.9 ± 0.4	174 ± 1	50 ± 1
	M4	6 ± 0.5	-1.4 ± 0.4	171 ± 5	90 ± 4	M4	7 ± 0.4	-2.9 ± 0.4	179 ± 4	86 ± 5
	M6	6 ± 0.4	-1.1 ± 0.4	225 ± 5	69 ± 5	M6	6 ± 0.5	-1.2 ± 0.6	217 ± 5	73 ± 6
	2MN6	4 ± 0.4	-1.1 ± 0.5	197 ± 5	66 ± 6	2MN6	5 ± 0.5	-0.8 ± 0.6	186 ± 7	69 ± 6
	S2	4 ± 0.4	-1.1 ± 0.4	221 ± 9	47 ± 8	MN4	4 ± 0.4	-2.0 ± 0.5	150 ± 11	76 ± 12
FB03	M2	28 ± 0.3	-2.0 ± 0.3	231 ± 1	40 ± 1	M2	25 ± 0.3	2.5 ± 0.3	223 ± 1	37 ± 1
	N2	6 ± 0.3	0.0 ± 0.3	203 ± 2	40 ± 3	M6	6 ± 0.3	0.1 ± 0.3	237 ± 3	37 ± 2
	M6	6 ± 0.2	0.6 ± 0.3	251 ± 3	48 ± 3	N2	5 ± 0.3	1.0 ± 0.3	205 ± 3	42 ± 4
	S2	5 ± 0.3	0.0 ± 0.3	255 ± 4	40 ± 4	S2	4 ± 0.3	0.3 ± 0.3	251 ± 4	40 ± 4
	2MN6	4 ± 0.2	0.4 ± 0.2	224 ± 4	51 ± 4	2MN6	4 ± 0.3	0.1 ± 0.3	208 ± 4	40 ± 4
WLIS	M2	27 ± 0.5	-5.0 ± 0.5	216 ± 1	26 ± 1	M2	19 ± 0.6	3.4 ± 0.4	199 ± 2	17 ± 1
	S2	6 ± 0.5	-0.8 ± 0.5	243 ± 5	25 ± 5	S2	4 ± 0.5	0.8 ± 0.4	230 ± 8	23 ± 7
	N2	5 ± 0.5	-1.1 ± 0.6	188 ± 6	23 ± 7	M6	4 ± 0.2	0.2 ± 0.2	218 ± 4	23 ± 3
	M6	4 ± 0.2	-0.1 ± 0.2	231 ± 4	25 ± 3	N2	3 ± 0.5	0.9 ± 0.4	166 ± 14	16 ± 11
	2MN6	2 ± 0.3	-0.0 ± 0.2	201 ± 7	24 ± 5	2MN6	2 ± 0.3	0.1 ± 0.2	189 ± 6	23 ± 5

10 to 15 percent that of M_2. At station BW, which has the longest record, the low-frequency constituent M_{SF}, which is a result of interactions between M_2 and S_2, is of comparable magnitude to L_2, although it is still only 2 cm s^{-1} in amplitude. Near bottom, the same set of frequencies dominate the records though the M_6 is slightly larger than the M_4 at station M02. The M_{SF} is not among the five largest constituents near the bottom at station BW.

In the western Sound, the M_2 tidal current amplitude decreases but it is still the largest constituent. In this area, the amplitudes of N_2 and S_2 are also approximately 25 percent of M_2, but the overtide amplitudes become larger relative to M_2, and M_4 and M_6 rank higher than N_2 and S_2 at some stations. $2MN_6$ and MN_4 also appear among the five largest species. MN_4 results from shallow water interactions between M_2 and N_2, and $2MN_6$ is a sixth diurnal tide resulting from M_4 interacting with N_2.

Tables 6 and 7 summarize the vertical structure of the M_2 tidal current ellipse properties in the eastern and western Sound, respectively. Note that FB03a represents the nearshore location of station FB03 during summer 2005 and FB03 represents the averages of all other deployments, as seen in Figure 3. This figure also shows the semi-major and semi-minor axes of the near surface and near bottom M_2 tidal current ellipses at all stations along with bathymetric contours. Figure 3 demonstrates that the M_2 tidal currents near the surface are very nearly along-Sound, and are more aligned with bathymetric contours near bottom. The amplitude, phase, orientation and ellipticity (defined as semi-minor axis over semi-major axis) of M_2 in the western Sound are also shown graphically in Figure 4. The values for Table 7 are averaged, while the figure displays individual deployments to reveal the degree of variability in the observations.

The near surface ellipses in the western-most stations (EXRCK and FB01-3) range between 36 and 47 degrees which is consistent with the geographic orientation of the thalweg of the Sound in this area. At the WLIS station Table 7 shows that the orientation of the near surface M_2 ellipse shifts to 24 degrees; at the BW station, in the central Sound, the orientation is almost exactly east-west. Stations M01-6 lie in a region of complicated bathymetry and this is reflected in the variability of the ellipse orientations among these stations. At M02, M05 and M06 the near surface ellipses are aligned within a few degrees of east but the M01 and M03 major axes parallel the local isobaths. Near bottom the orientation of the current ellipses appears to be more influenced by the bathymetry. This is particularly evident at EXRCK where the current meter is located on the flank of a deep channel and the ellipse orientation changes significantly from the direction of the axis of the Sound at the surface to align with the bathymetry near the bottom.

The magnitudes of the ellipticity of the M_2 harmonic in the western Sound are listed in Table 7. Values tend to be small and negative (indicating anticyclonic rotation) near the surface, but close to the bottom they are positive and the magnitudes increase substantially. Station FB03a is anomalous in the sense that the ellipticity is almost uniform and negative throughout the water column, with an average value of -0.25. In the central and eastern Sound the estimates of the ellipticy (see Table 6) at stations M01, M03 and BW show the same general pattern, small negative values in the upper water column and positive values

Table 6. M_2 properties at eastern Long Island Sound stations as a function of depth. Values are seasonally averaged to represent the mean characteristics for each station. Properties are the same as those explained in Figure 5.

	Depth (m)	Amp (cm s^{-1})	Phase (deg)	Orientation	Ellipticity
BW	3	37 ± 0.6	242 ± 1	181 ± 1	−0.07
	6	37 ± 0.6	242 ± 1	181 ± 1	−0.06
	9	37 ± 0.5	242 ± 1	180 ± 1	−0.05
	12	37 ± 0.5	240 ± 1	179 ± 1	−0.04
	15	36 ± 0.5	238 ± 1	177 ± 1	−0.02
	18	35 ± 0.5	234 ± 1	175 ± 1	0.01
	21	34 ± 0.5	228 ± 1	172 ± 1	0.07
	24	31 ± 0.5	224 ± 1	171 ± 1	0.14
	27	28 ± 0.5	221 ± 1	171 ± 1	0.17
M01	3	65 ± 6.4	231 ± 6	34 ± 6	−0.11
	6	63 ± 4.7	230 ± 5	32 ± 5	−0.08
	9	59 ± 5.3	228 ± 5	31 ± 4	0.01
	12	54 ± 5.0	225 ± 6	30 ± 5	0.12
	15	47 ± 4.5	221 ± 6	29 ± 6	0.23
	18	43 ± 4.5	218 ± 6	29 ± 6	0.28
M02	3	74 ± 6.2	229 ± 5	1 ± 2	−0.12
	6	72 ± 3.4	226 ± 3	2 ± 2	−0.11
	9	68 ± 2.7	222 ± 2	3 ± 2	−0.09
	12	62 ± 2.8	220 ± 3	4 ± 2	−0.05
	15	56 ± 2.6	218 ± 3	5 ± 3	−0.03
	18	52 ± 3.0	217 ± 3	5 ± 2	−0.02
M06	3	70 ± 6.6	227 ± 5	2 ± 2	−0.11
	6	69 ± 6.7	226 ± 5	3 ± 2	−0.10
	9	66 ± 4.5	225 ± 4	4 ± 2	−0.09
	12	63 ± 4.2	224 ± 4	4 ± 2	−0.09
	15	58 ± 4.2	223 ± 4	5 ± 2	−0.08
	18	54 ± 4.1	222 ± 4	5 ± 2	−0.07
M03	6	89 ± 9.0	233 ± 6	22 ± 6	−0.19
	9	86 ± 6.7	233 ± 5	22 ± 4	−0.14
	12	82 ± 5.9	233 ± 4	21 ± 3	−0.09
	15	78 ± 5.2	233 ± 4	21 ± 4	−0.04
	18	73 ± 5.9	233 ± 4	21 ± 4	0.01
	21	68 ± 5.2	233 ± 4	22 ± 4	0.06
	24	62 ± 4.2	232 ± 4	23 ± 4	0.11
	27	56 ± 3.8	231 ± 4	24 ± 5	0.18
	30	50 ± 4.0	230 ± 5	25 ± 5	0.22
M05	3	69 ± 7.1	211 ± 6	177 ± 4	−0.04
	6	67 ± 7.3	210 ± 6	179 ± 3	−0.05
	9	63 ± 5.3	209 ± 4	1 ± 2	−0.06
	12	58 ± 4.3	208 ± 5	2 ± 3	−0.07
	15	51 ± 3.5	207 ± 4	3 ± 4	−0.07

Table 7. M_2 properties at western Long Island Sound stations as a function of depth. Values are seasonally averaged to represent the mean characteristics for each station. Properties are the same as those explained in Figure 5.

	Depth (m)	Amp (cm s^{-1})	Phase (deg)	Orientation	Ellipticity
EXRCK	3	18 ± 0.4	247 ± 1	40 ± 1	0.01
	6	16 ± 0.3	236 ± 1	39 ± 1	0.01
	9	15 ± 0.3	232 ± 1	41 ± 1	0.08
	12	14 ± 0.2	234 ± 1	49 ± 1	0.16
	15	13 ± 0.2	230 ± 1	56 ± 1	0.30
FB01	3	24 ± 0.4	231 ± 1	42 ± 1	−0.02
	6	23 ± 0.3	229 ± 1	43 ± 1	0.03
	9	21 ± 0.3	225 ± 1	44 ± 1	0.11
	12	19 ± 0.3	218 ± 1	45 ± 1	0.22
FB02	3	24 ± 0.4	235 ± 1	39 ± 1	−0.10
	6	23 ± 0.3	235 ± 1	40 ± 1	−0.05
	9	22 ± 0.5	232 ± 1	39 ± 1	0.04
	12	19 ± 0.4	222 ± 1	34 ± 1	0.23
	15	16 ± 0.3	210 ± 2	31 ± 2	0.43
FB03a	3	20 ± 0.5	194 ± 2	47 ± 2	−0.28
	6	19 ± 0.5	188 ± 2	49 ± 1	−0.28
	9	17 ± 0.4	178 ± 2	49 ± 2	−0.25
	12	14 ± 0.2	156 ± 1	55 ± 1	−0.20
FB03	3	28 ± 0.3	232 ± 1	40 ± 1	−0.07
	6	28 ± 0.3	231 ± 1	40 ± 0	−0.06
	9	27 ± 0.3	228 ± 1	37 ± 1	0.00
	12	24 ± 0.3	223 ± 1	37 ± 1	0.11
WLIS	3	28 ± 0.6	217 ± 1	26 ± 1	−0.20
	6	26 ± 0.4	216 ± 1	27 ± 1	−0.15
	9	24 ± 0.4	214 ± 1	25 ± 1	−0.06
	12	21 ± 0.5	207 ± 1	21 ± 1	0.06
	15	19 ± 0.6	200 ± 2	17 ± 1	0.18
BW	3	37 ± 0.6	242 ± 1	57 ± 1	−0.07
	6	37 ± 0.6	242 ± 1	58 ± 1	−0.06
	9	37 ± 0.5	242 ± 1	57 ± 1	−0.05
	12	37 ± 0.5	240 ± 1	56 ± 1	−0.04
	15	36 ± 0.5	238 ± 1	142 ± 1	−0.02
	18	35 ± 0.5	234 ± 1	138 ± 1	0.01
	21	34 ± 0.5	228 ± 1	136 ± 1	0.07
	24	31 ± 0.5	224 ± 1	171 ± 1	0.14
	27	28 ± 0.5	221 ± 1	172 ± 1	0.17

near the bottom. However, the three more northerly stations, M02, M05 and M06, show small negative ellipticity values at all depths.

In the western Sound the phase of the near surface M_2 currents varies little with longitude and the currents at WLIS lead EXRCK by approximately 20 degrees or 40 minutes. Vertical variations in the phase have similar magnitudes at most stations with the bottom currents

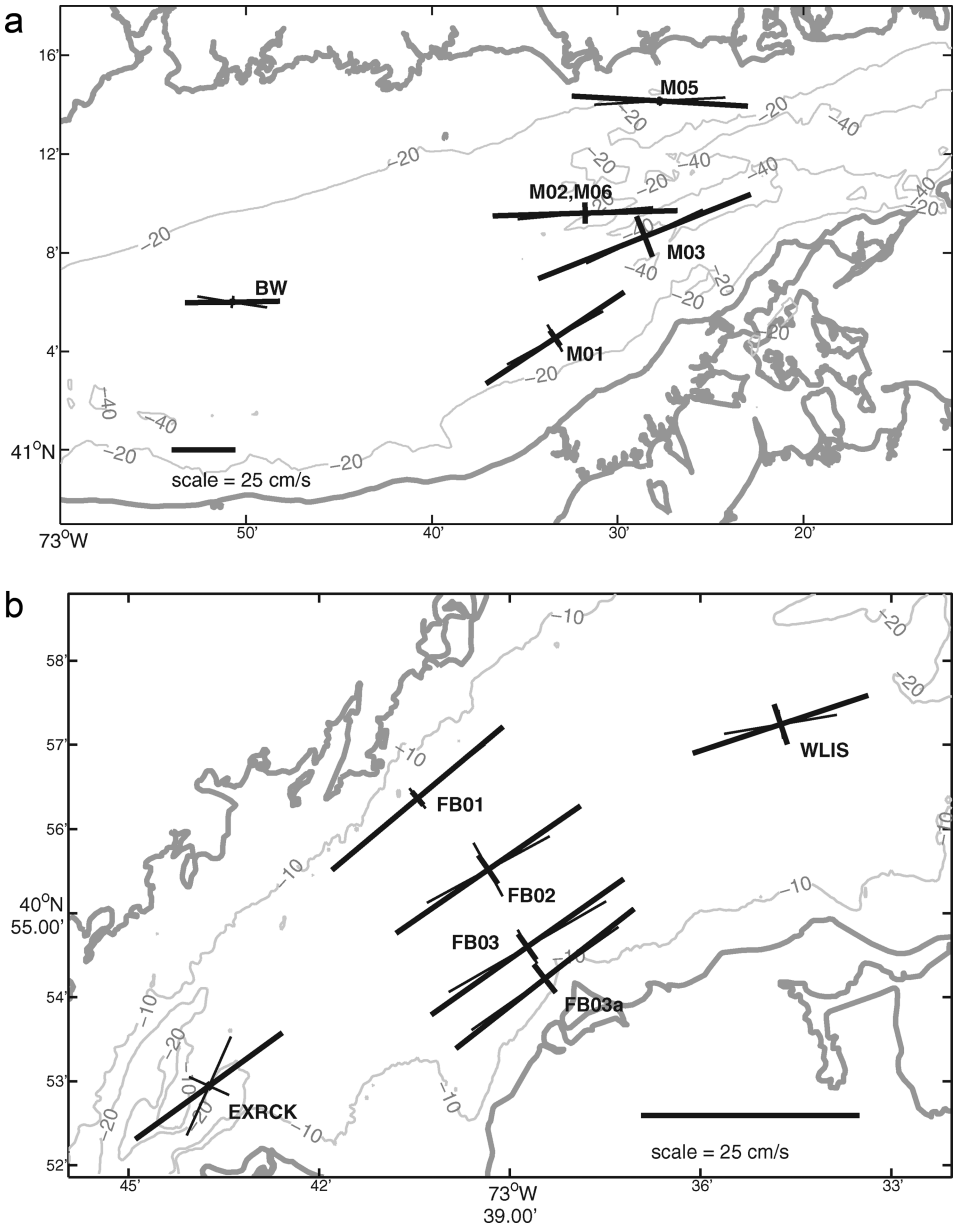

Figure 3. M_2 tidal ellipses at 3 m depth (heavy line) and near bottom (light line) for ADCP deployments in the eastern (a) and western (b) Sound. Semi-major and semi-minor axis amplitudes are shown centered at the location of the deployment. Note the different velocity scales for the two figures.

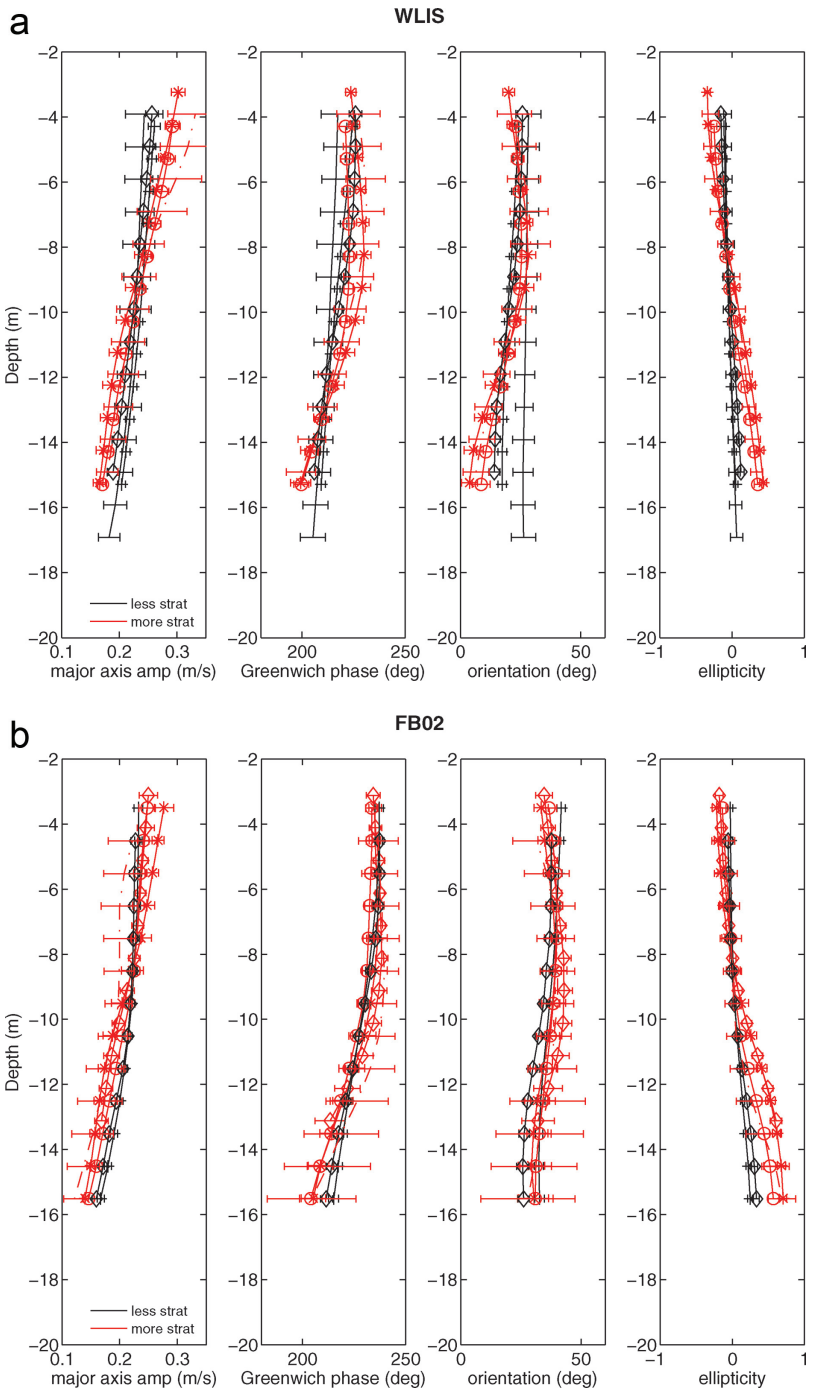

Figure 4. (Continued)

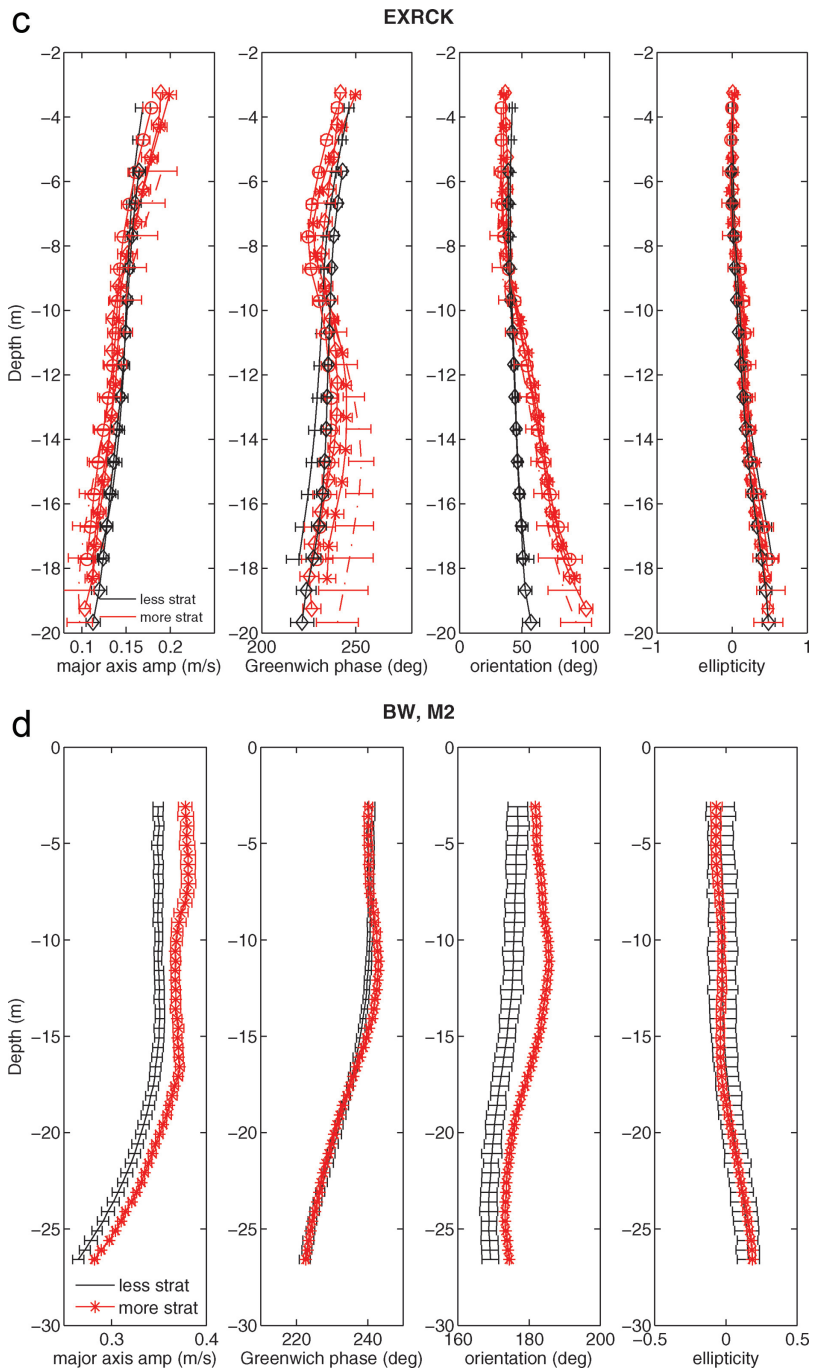

Figure 4. M_2 ellipse characteristics for western and central Sound deployments, shown by station (a-d). Displayed are the major axis amplitude, Greenwich phase and orientation in degrees, and ellipticity (minor axis amplitude / major axis amplitude). Analysis was performed separately during more stratified ($\Delta\rho > 1\,\mathrm{kg\,m^{-3}}$ in the west, and $\Delta\rho > 0.5\,\mathrm{kg\,m^{-3}}$ at station BW), and less stratified conditions (represented by red and black lines, respectively). Note that there were more individual deployments in the western Sound (a–c) relative to the central Sound (d).

leading the surface currents. Station FB03a shows the most anomalous behavior; the near surface phase there precedes WLIS by 30 degrees and the vertical variation at the station is almost 40 degrees. Even more remarkable is the phase difference between the surface currents at FB03a and FB03b; 40 degrees difference at the surface and 65 degrees at 12 m. This implies considerable lateral and vertical shear in this region.

Among the central and eastern Sound stations the phase variation in the horizontal is very small with currents at the shallower sites leading. The most significant difference is at M05, which is in shallow water north of Long Sand Shoal. There, currents lead the southern stations by approximately 20 degrees at all depths. The phase lag between the nearshore stations and those along the Sound's axis is larger than the lag between the BW and M01. This is consistent with the idea that the M_2 tide in the Sound is nearly a standing wave. The largest vertical phase difference is at the central station, BW, where there is a 20 degree lag between the tidal velocities at 3 meters and 27 meters. To the east, where currents are more vigorous and the bathymetry complex, phases vary in the vertical at each station by only 3 to 13 degrees.

Since the current observations in the western Sound and at BW were acquired during both the summer and winter, we can assess the potential influence of seasonal variations in vertical stratification on the structure of the principal tidal current constituent, M_2. We employed the measurements of the CTDEP hydrographic survey program (Kaputa and Olsen, 2000), at their stations A4 (near EXRCK) and H4 (near BW) to describe the evolution of the density field, and divided the ADCP records into high and low stratification intervals. In the western Sound a threshold of 1 kg m^{-3} density difference between surface and bottom was used, and a greater than 0.5 kg m^{-3} difference was considered high stratification in the central Sound. The different thresholds are a result of the decreasing level of stratification moving toward the eastern Sound (Fig. 2), and the minimum stratification at each site was chosen based on the seasonal climatology at that location so that a typical winter density profile would be classified relatively less stratified and a typical summer profile more stratified. Harmonic analysis was applied to estimate the current ellipse parameters for intervals longer than 13 days. The vertical structure of the M_2 ellipse parameters at stations FB01 and FB03 did not show significant or consistent differences with the level of stratification; therefore, we only discuss the analyses at the other sites.

Figure 4a shows the vertical structure of the semi-major axis amplitude, phase, orientation and ellipticity at WLIS with the estimates from more stratified periods shown in red. Though the magnitudes of the uncertainty are comparable to the differences between the more and less stratified amplitudes, it is evident that the vertical gradient of the major axis amplitude is enhanced during the more stratified intervals. The estimates also reveal changes to the vertical structure of the phase. During the less stratified periods the phase difference between the top and bottom bin averages approximately 20 degrees, and the gradient is almost uniform. During the more stratified intervals, however, the phase changes approximately 25 degrees in the bottom half of the water colum, and is nearly uniform in the upper half. When the water column is more stratified the orientation is closer to zero

in the lower water column, tilting the tidal ellipse clockwise, and the ellipticity increases substantially at the bottom and decreases at the surface. The difference in the structure of the ellipse parameters between stratified and unstratified periods at station FB02 is illustrated in Figure 4b. With the exception of the orientation angle, the changes are similar to those at WLIS.

At EXRCK Figure 4c shows that increased stratification is again associated with a slight increase in the vertical shear of the semi-major axis and more structure in the vertical variation of the phase. The most dramatic difference, however, is in the ellipse orientation in the lower half of the water column during the more stratified periods; an increase by almost 40 degrees at the bottom is evident. At this station the instrument is located on the side of the channel leading to the East River and it appears that increased stratification leads to an alignment of the lower level current with the topography. There is no visible change in ellipticity with stratification at this location.

Finally, at station BW in the central Sound (Fig. 4d), periods of higher stratification cause an increase in the amplitude of the semi-major axis and and an increase in the orientation at all depths, tilting the tidal ellipse clockwise. At this station there is no significant change in the phase or ellipticity due to increasing stratification.

The relatively large amplitude of the overtides in the western Sound was a suprising result of our analyses and we presume this is a signature of the importance of nonlinear mechanisms in that region. Figures 5a and 5b show the semi-major and semi-minor axis amplitude and phase of the M_4 constituent at the eastern and western ADCP stations respectively. Values are the average of all deployments at each station. The amplitudes range from 1–6 cm s^{-1} with the largest values occuring at M03 in the eastern Sound. This station also has a strong minor axis component near the surface, of similar magnitude to the major axis amplitude, indicating that M_4 is highly influenced by rotation at this location. There is no consistent pattern to the depth structure of the amplitudes, and the phases also show no clear depth structure.

The higher frequency M_6 component's amplitude and phase are shown in Figures 5c and 5d. These amplitudes are higher than M_4 in the western Sound and of comparable magnitude in the eastern and central Sound. Again, amplitudes display minimal vertical structure. Phases have some consistency between stations in the western Sound and are more variable to the east.

The depth-averaged M_4 velocity amplitudes are highest in the eastern Sound where the maximum was 3.8 cm s^{-1} at station M03. In contrast, values in the central and western basins were closer to 1.0 cm s^{-1}. The M_6 velocities show the opposite trend, with a maximum value of 4.1 cm s^{-1} in the western Sound, a minimum of 0.2 cm s^{-1} at the central Sound station, and a range from 1.2 to 2.7 cm s^{-1} to the east. Therefore, while the M_4 velocities decrease from east to west in a manner similar to the M_2 velocities, the M_6 velocities are relatively larger in the western end of the Sound.

Since overtides are generated by nonlinear processes, it is not surprising that they have higher amplitudes in the western Sound where the estuary narrows and shoals. The along-Sound variation of the ratio of the M_4 and M_6 amplitudes, and the secondary semidiurnal

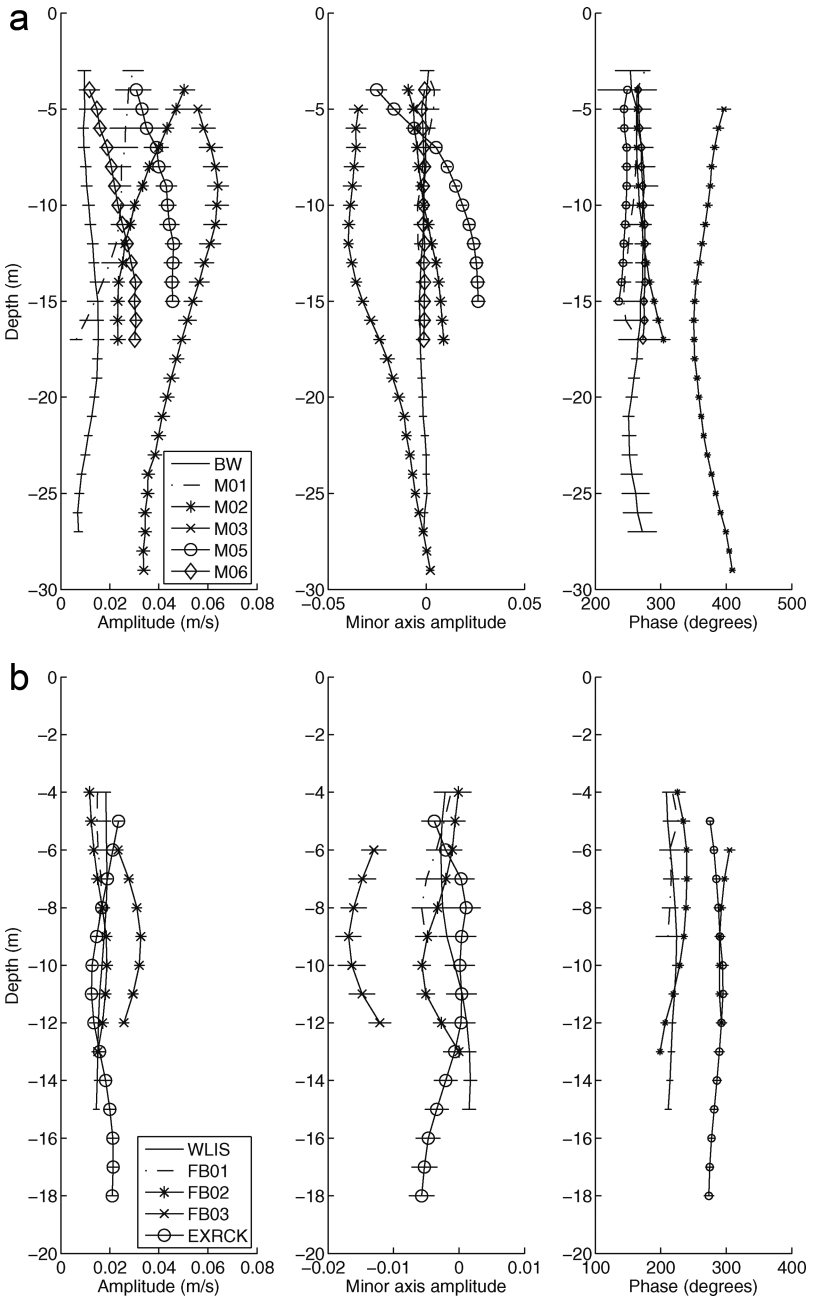

Figure 5. (Continued)

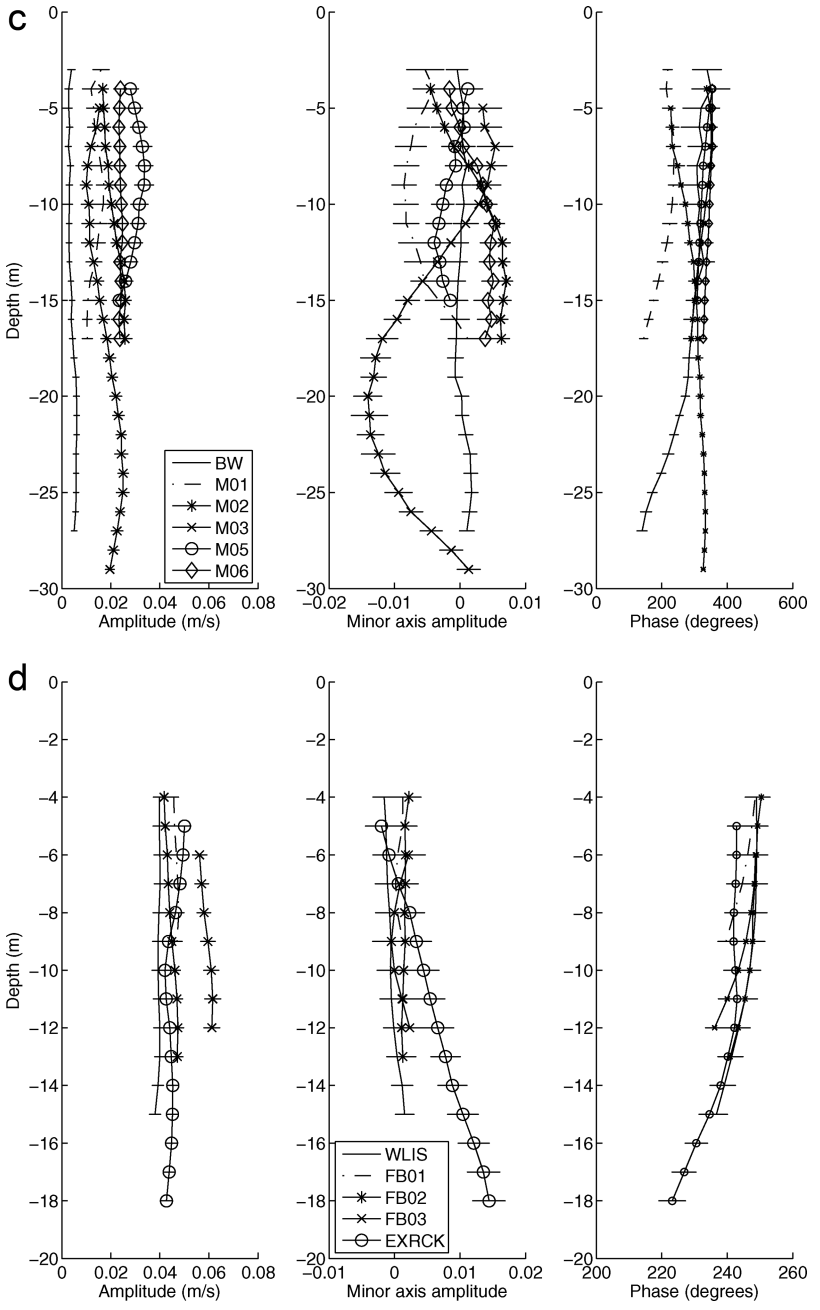

Figure 5. Tidal amplitudes and phases as a function of depth for the constituents M_4 (a and b) and M_6 (c and d) at all stations. Amplitudes and phases are averaged over all deployments at each location.

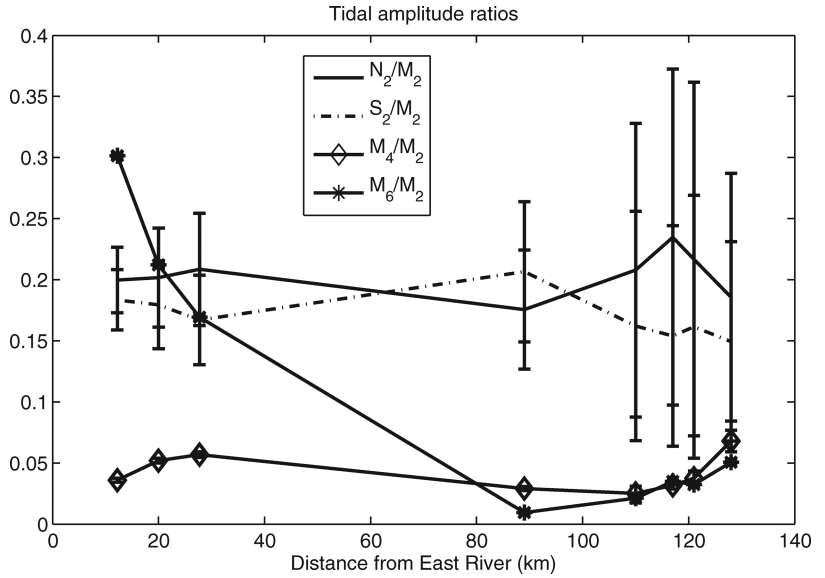

Figure 6. Along-sound variation of depth mean semidiurnal tidal constituents and overtides relative to M_2 from summer 2007.

constituents N_2 and S_2, to the M_2 are displayed in Figure 6. The semidiurnal constituents are 15–25 percent of the M_2 amplitude throughout the Sound, showing no along-estuary trend, and the variation of the relative magnitude of M_4 is weak. However, M_6 is significantly amplified in the western Sound, where it becomes larger than the secondary semidiurnal constituents. The mechanism responsible for this phenomenon is uncertain, and the subject of on-going work.

Finally, it is important to note that when the tidal signal is removed from the velocity records, a subtidal flow is revealed. In the western Sound, this flow is generally to the east (toward the mouth) near the surface and to the west (toward the head) at depth. The net flow is toward the East River (Gay *et al.*, 2004). This subtidal flow is important, as it can be partially generated by tidal flows, and can also affect the magnitude of overtides.

5. Discussion

The results presented in the previous section provide the first extensive description of the vertical and along-Sound structure of the tidal currents in Long Island Sound. In this section we compare the vertical structure of the M_2 constituent to two simple analytic models and comment on the influence of seasonal variations in the vertical density gradient. We then compare the observed horizontal variation of the amplitude of the M_2 constituent to the predictions of a one-dimensional, nonlinear layer model with variable channel width and depth. Since the nonlinear terms in this model generate overtides, we compare the structure

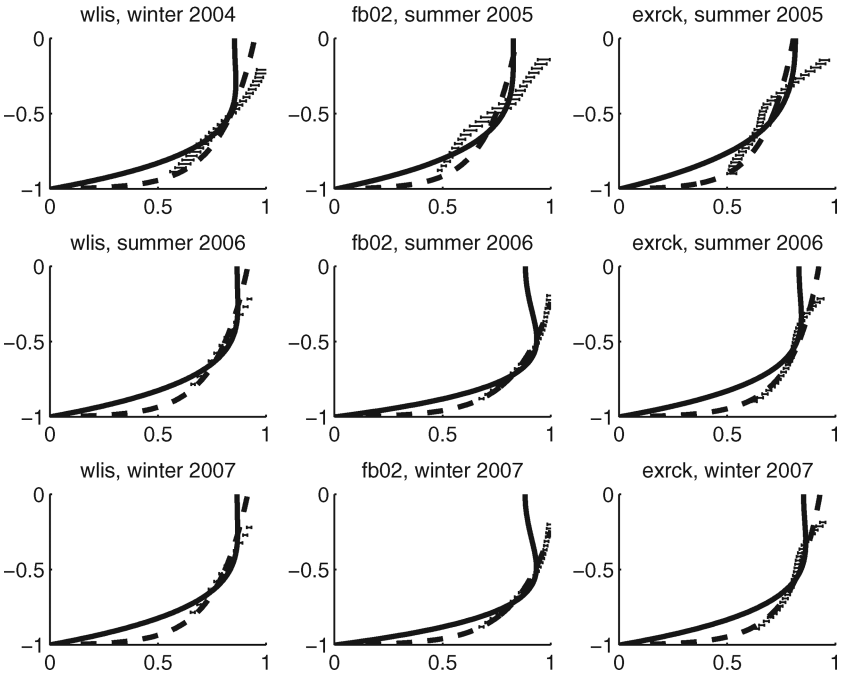

Figure 7. Tidal current amplitudes (thin line with error bars), normalized to the surface, compared to the analytical model results (thick line) for the constant viscosity case (solid) and the parabolic viscosity case (dashed) with the parabolic maximum at mid-depth and the frictional depth adjusted to produce the best fit. Error bars on data are one standard deviation.

of the predicted amplitudes to observations and comment on the effect of the mean flow through the Sound.

a. Vertical structure of the M_2

In Section 3a we summarized the theory of Ianniello (1977a,b). We then compared his constant viscosity model to examples of the observed vertical structure of the M_2 amplitudes and phases in the western Sound over three deployments at stations WLIS, FB02 and EXRCK. These stations are near the central axis of the Sound and least sensitive to the local effects of coastal boundaries; therefore, they provide the best comparison to the one-dimensional models. The results of these comparisons for the constant viscosity case are shown in Figure 7, in which the tidal velocity data (normalized to the surface) is shown by the thin line with error bars, and the amplitude of the constant viscosity model is represented by the solid line. For each station and sampling effort, the eddy viscosity (and therefore the frictional depth) has been adjusted to produce the best fit with the model in question.

Comparison of the model predictions with the estimates of the major axis amplitudes shows that, though they have the same decreasing trend with depth below the surface, most (more than 90 percent) of the estimates are separated from the model prediction by more than one standard deviation. The phases (not shown here) are also inconsistent. Consequently, we must conclude that the model is flawed. We also evaluated the solution of Winant (2007), to assess whether the contributions of the Coriolis effect were the cause of the poor model performance. However, we found that the predicted across-sound tidal amplitudes were even less consistent with the data than the along-Sound amplitudes, and the along-sound solution was indistinguishable from the nonrotating case for the parameters appropriate to Long Island Sound. This does not imply that rotation is not important in Long Island Sound, rather it confirms that our one-dimensional model is still oversimplified given the complexities of the system.

Several potential explanations for the failure of the model are plausible. One is that the model neglects the details of the bathymetry and coastal geometry. However, since the model failed to describe the amplitude structure at any of the sites we regard this as unlikely. As proposed by Ianniello (1977a,b) and others, the vertical eddy viscosity may vary with distance from the surface and bottom boundaries. To evaluate this possibility we adopted a parabolic form for $A_z(z)$. The observations of amplitude and phase were not consistent with this version of the model for any of the deployments. If only the vertical structure of the amplitude is used, then the model and data agree for the summer of 2006 and winter of 2007 at station FB02 (see the dashed line in Fig. 7). However, this agreement relies on an erroneously high vertical eddy viscosity of order $1\ \mathrm{m^2\ s^{-1}}$. Ignoring the vertical structure of the phase therefore has the potential to be very misleading since it can lead to estimates of the eddy viscosity that are three orders of magnitude larger than estimates in the literature. This comparison of model results and observations demonstrates that the model is inadequate in all cases when both the predicted amplitude and phase are taken into account.

b. The influence of stratification

In Section 4, we noted that the vertical profile of the M_2 tidal ellipse could be separated by high and low stratification conditions, as shown in Figure 4. The tidal amplitude, phase, orientation and ellipticity were all affected by stratification for at least one of the stations in the central and western Sound. We, therefore, investigate possible mechanisms for this observation.

For the semidiurnal tidal constituents in Long Island Sound, the ratio of δ_+/δ_- is 0.44, implying that the frictional layer of the anticyclonic component is almost twice that of the cyclonic component. To estimate these depths, a value must be chosen for A_z. Using the simple empirical formula of Bowden and Fairbairn (1952), $A_z = 2.5 \times 10^{-3} h_0 U_{1R}$ where h_0 is the maximum water depth and U_{1R} is the tidal velocity, we obtain an estimate of A_z for the western Sound of $9 \times 10^{-3}\ \mathrm{m^2\ s^{-1}}$, using a depth of 18 meters and a velocity of $20\ \mathrm{cm\ s^{-1}}$. This value is similar to those obtained for the magnitude of the eddy viscosity

using the uniform viscosity version of the model of Ianniello (1977a, 1977b). This estimate suggests that the anticyclonic rotary component of the M_2 tide is influenced by friction over 19.7 meters, most of the water column, while the cyclonic component is only modified by bottom friction in the lower half of the water column. Following the argument of Souza and Simpson (1996), enhanced stratification should result in a larger amplitude anticyclonic current component at the surface (negative ellipticity), and a reduced amplitude cyclonic component at depth (positive ellipticity). This behavior was observed at stations WLIS and FB02 (Figs. 4a and 4b), as noted in the previous section, suggesting that the reduction in vertical turbulent transport by stratification is significant in western Long Island Sound. However, Figures 4c and 4d show that there is no significant change in the ellipticity between more and less stratified seasons at EXRCK or BW; only the orientations appear to be modified at these locations. The local effects of stratification on friction alone can't explain these observations; therefore, a much more sophisticated theoretical analysis is warranted.

c. Overtide generation

Our analysis of velocity observations has shown that the tidal velocity of the semidiurnal constituents in the Sound decreases from east to west. This is broadly consistent with the predictions of linear models with frictional dissipation like those of Kenefick (1985) and Bogden and O'Donnell (1998). However, these models do not predict the structure of the observed overtides, M_4 and M_6. As shown in Figure 6, the magnitude of the M_6 component is amplified relative to M_2 in the western Sound. In Section 3b, we summarized the model of Parker (1984), who described how the shelf-forced tide and its nonlinear interaction with mean flow due to a river generate overtides in Delaware Bay. To assess whether the dynamics in this model can describe the structure of the tides in the Sound, we compare the model predictions to the observations discussed in Section 4.

Our numerical implementation of the Parker (1984) model (as described in Eqs. 6 and 7) follows his approach. We chose to specify the sea level at the Race, the junction of Long Island Sound and Block Island Sound, and to simulate the flow between there and the East River 140 km to the west. The mean cross-sectional depth is used to approximate a rectangular basin, and this depth varies linearly along the axis of the Sound. The estuary breadth is a piecewise linear representation of the more complex along-estuary variations in width.

The time series $\eta_R(t)$ is synthesized using estimates for the amplitude and phase of the M_2, N_2, S_2, K_1 and O_1 sea level constituents normalized to the values of M_2 at the New London station. As the model's eastern boundary is to the west of New London, the absolute magnitude of the M_2 amplitude and phase are interpolated to the boundary's location. At the East River (*ER*) boundary we employ three alternative conditions: either no flow, $u(x = 0, t) = u_{ER}(t) = 0$, or prescribed sea level, $\eta(x = 0, t) = \eta_{ER}(t)$, treated in two ways. For the first prescribed sea level case, we set $\eta_{ER}(t) = \eta_{semi}(t) + \Delta\eta$ where $\eta_{semi}(t)$

is computed using semidiurnal and diurnal amplitude and phase estimates from Kings Point and $\Delta\eta = 0.034$ m, the difference between the mean sea level across the model domain. For the second case where sea level is imposed at $x = 0$, we set $\eta_{ER}(t) = \eta_{ot}(t) + \Delta\eta$, where η_{ot} is η_{semi} with the addition of the M_4 and M_6 constituents. Adding the M_4 and M_6 constituents to the boundary forcing at the eastern end did not fundamentally change the model results, and their addition at the western end allows representation of overtides generated within the East River to propagate into the model of the Sound. These options allow tidal flow through the East River, enabling us to evaluate the influence of a steady transport within the Sound on the structure of the tide and overtide amplitudes. The value for $\Delta\eta$ was chosen to produce a volume flux at the western end of 500 $m^3\,s^{-1}$, which is roughly consistent with the estimate of Blumberg and Pritchard (1997) of 310 $m^3\,s^{-1}$.

The model contains 50 grid points between the East River and the Race; comparisons with the analytic model showed that a denser grid did not provide significant improvement in the solution and greatly increased the run time. Model runs spanned eight tidal cycles, with the first four considered spinup and the last four used in the harmonic analysis of the results. The time step depends on the frictionless wave speed, a function of estuary depth. The frictional coefficient in the model, C_D, is set to a constant 0.002 for all locations.

The transport through the Sound has no discernable influence on the predicted sea level distribution, however it does increase the phase difference across the domain, leading to closer agreement with the observed values near the western boundary. The agreement between the model's sea level M_2 amplitude and phase distributions and the observations are surprisingly good, especially considering that the model geometry only represents the largest scale structures, that there is only one adjustable parameter, C_D, and that we compare the across-Sound average sea level to measurements at single points. The discrepancy is largest for the central Sound ADCP comparisons in the eastern Sound, where the ADCP backscatter estimates appear to be biased low.

The simulated distribution of the vertically averaged M_2 current amplitude was compared to our observations at stations near the center of the Sound, as well as to values reported by Gordon and Pilbeam (1975) and Cobb *et al.* (1978), which were at a fixed depth. There is very little difference between the three solutions except near the western boundary where the predicted amplitudes for the cases forced by sea level are slightly larger and more consistent with the observations. Again, the model predictions and observations overall are very consistent.

For the vertically averaged M_4 velocity amplitudes, the best agreement is with the no-flow case, as seen in Figure 8 where the top panel shows the ratio of M_4 to M_2 and the no-flow case is the solid red line. The velocity ratios obtained from data are shown in black. When the boundary is opened (dashed line), M_4 velocities are amplified most notably at the western end of the model, and this is only slightly reduced when overtides are added to the forcing at the East River (pluses). By increasing the mean flow we were able to decrease the M_4 amplitude, but even a sea level difference across the domain of 10 cm, corresponding to a mean westward flow of 62 cm s^{-1} at the East River, was insufficient to

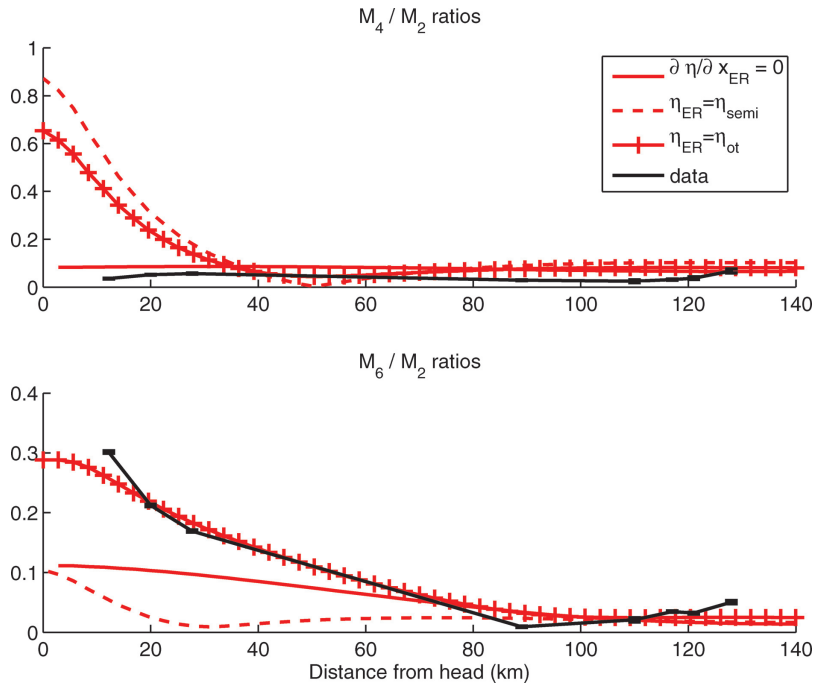

Figure 8. Ratio of M_4 and M_6 depth-averaged velocities to M_2 for the three model cases (red) and for the data (black) as a function of distance along the estuary. This shows that no single model case is in good agreement with the data in the western Sound for both M_4 and M_6.

bring the predictions into agreement with the data. Therefore the model, in its current form, is incapable of representing the M_4 velocities measured in the western Sound.

As for M_6 (Fig. 8, bottom panel), the no-flow case overestimates its amplitude in the central Sound, and underestimates it in the western Sound velocities. When sea level forcing at the diurnal and semidiurnal frequencies is added, the along-Sound structure is modified, but it remains inconsistent with the data. Adding overtides to the sea level forcing at the East River increases the M_6 velocity amplitude throughout the Sound and is much more consistent with mooring estimates in the western Sound. However, the model continues to overestimate M_6 in the central Sound, where its measured value is close to zero.

In summary, the model with sea level forced at both ends by M_2, N_2, S_2, K_1 and O_1 and with M_4 and M_6 added at the western end can successfully reproduce measured sea level amplitude and phase and depth-averaged M_2 velocity throughout the Sound. While the model includes the generation of higher frequency harmonics through nonlinear interactions, it can't produce accurate M_6 velocities at the converging western end of the Sound unless the overtides generated within the East River are added to the boundary forcing. The nonlinear processes in the model also generate the M_4 constituent; however, the mean flow

and boundary forcing required to produce a reasonable representation of M_6 degrades the simulation of M_4. The M_4 to M_2 ratio is constant when the East River is a closed boundary, and when the boundary is opened M_4 is reduced in the central Sound and amplified to the west. In contrast, M_6 is largest relative to M_2 with an open boundary and sea level forcing at the M_4 and M_6 frequencies. Something is clearly missing in the model. It is possible that the model geometry is too simple and that neglecting smaller scale features eliminates a critical source of nonlinear overtide generation. Alternatively, the vertical structure of the currents and the interaction between stratification and bathymetry, which would appear in the model as time variation in the friction term, may be critical.

6. Summary and conclusions

We have presented a set of velocity and sea surface level observations from Long Island Sound that resolves both along-Sound and water column variations in tidal velocities. These data are an important resource with which both analytic and numerical models can be evaluated. The most unexpected result of our analysis is the discovery of relatively large amplitude M_6 overtides in the western Sound and weak M_4 amplitudes. Since these are signatures of nonlinear dynamics, simulating the magnitude and spatial structure of these constituents will pose a sensitive test of numerical circulation models.

By comparing modeled predictions of the vertical structure of the principal tidal current constituent (M_2) using both constant and parabolic vertically varying eddy viscosities to the amplitude and phase estimates obtained from measurements, we demonstrated that both models must be rejected as inconsistent with observations. Since we used observations at five sites throughout the western Sound spanning both summer and winter, we doubt that this result is a consequence of the local geometry or variations in stratification. We conclude that a more sophisticated representation of vertical turbulent transport in Long Island Sound is essential at the leading order of approximation. This result implies that models which use either vertically constant or varying, but time-invariant, eddy viscosities may be adequate for the prediction of tidal sea surface amplitudes and phases along with depth-averaged velocities, but are fundamentally insufficient for the prediction of tidal currents as a function of depth. We are aware that the eddy viscosity itself has been shown to vary over tidal cycles, but these same investigations have often found that while Reynolds stresses vary over a tidal cycle, they co-vary with velocity, and even taking this into account the velocities can often be modeled using a steady-flow model (Peters and Bokhorst, 2001; Rippeth *et al.*, 2002). As a result, our finding that the time invariant viscosity model is insufficient to reproduce our velocity data is worthy of note and further investigation.

We also tested a laterally and vertically averaged, nonlinear barotropic layer model of the circulation in a rectangular channel with cross-sectional area variation approximating the large-scale structure of Long Island Sound. Though the bottom friction coefficient can be selected so that the model predicts distributions of the M_2 amplitude and phase for both sea level and current that are consistent with the observations, the predicted structure of the M_4

and M_6 overtides are much more difficult to reproduce. When the model channel is closed at the East River, the M_4 simulation is acceptable but M_6 is underestimated. When sea level is specified at the East River and a realistic mean flow through the Sound is allowed, the simulation of the M_6 is improved but the M_4 is over-amplified. Since the nonlinear terms in the model generate overtides and mean flow, we conclude that either; (1) they are not adequately represented in layer models and the vertical structure, and its along channel variation are critical; (2) the simplification of the geometry distorts the relative importance of the fricional and advective nonlinearities; and/or (3) the representation of friction by a constant bed stress coefficient is inadequate. Therefore, any evaluation of nonlinear tidal constituents must include a more sophisticated model than the one presented here, and our current intuition for the mechanisms behind the nonlinearly generated overtides must be re-evaluated in light of these discoveries.

Since we have shown that the vertical structure of the principal tidal constituent is not described adequately by the time-independent eddy coefficient model in Long Island Sound, and that a nonlinear layer model does not produce acceptable simulations of the overtides, we conclude that these models must only be used for pedagogical purposes. They illustrate important mechanisms and interactions, and they also isolate what is unknown. Parker (1984) explained how the nonlinearities in the layer model led to overtides and rectification, however, unsteady eddy viscosity and along-channel variations in the vertical structure of the principal tidal constituent have a similar effect. To isolate the source of the overtides in the western Sound requires a detailed examination of these effects in a realistic three-dimensional model of the circulation in Long Island Sound and the East River.

Acknowledgments. The operation of the Long Island Sound Integrated Coastal Observing System (LISICOS) and the analysis presented here were supported by the National Oceanic and Atmospheric Administration through award NA04NOS4730256. The National Science Foundation supported the ADCP deployments in the eastern Sound through grant OCE-9634495. We thank Peter Gay for providing the figure detailing the along-Sound density structure in Long Island Sound.

This paper is dedicated to the memory of Rich Garvine to honor his commitment to his students and education.

REFERENCES

Andersen, O., G. Egbert, S. Erofeeva, and R. Ray. 2006. Mapping nonlinear shallow-water tides: a look at the past and future. Ocean Dynam., *56*, 416–429.

Blumberg, A. F. and B. Galperin. 1990. On the summer circulation in New York Bight and contiguous estuarine waters, in Residual Currents and Long-Term Transport, R.T. Cheng, ed. Springer-Verlag, 451–468.

Blumberg, A. F. and D. W. Pritchard. 1997. Estimates of the transport through the East River. J. Geophys. Res., *102*, 5685–5703.

Bogden, P. S. and J. O'Donnell. 1998. Generalized inverse with shipboard current measurements: Tidal and nontidal flows in Long Island Sound. J. Mar. Res., *56*, 995–997.

Bowden, K. and L. Fairbairn. 1952. A determination of the frictional forces in a tidal current. Proc. Royal Soc. London, Series A, Mathematical and Physical Sciences, *214*, 371–392.

Bowman, M. J. 1976. The tides of the East River, New York. J. Geophys. Res., *81*, 1609–1616.
Breaker, L., W. Broenkow, W. Watson, and Y. Jo. 2008. Tidal and nontidal oscillations in Elkhorn Slough, CA. Estuaries Coast., *31*, 239–257.
Cobb, S., P., J.R. Reese, M.A. Granat, B.W. Holliday, and E.H. Klehr. 1978. Aquatic disposal field investigations at Eatons Neck disposal site, Long Island Sound. An environmental inventory. AD-A-055217, Army Engineer Waterways Experiment Station, Vicksburg, MS, 125 pp.
Codiga, D. L. and L. V. Rear. 2004. Observed tidal currents outside Block Island Sound: Offshore decay and effects of estuarine outflow. J. Geophys. Res, *109*, doi:10.1029/2003JC001804.
Dean, R. and R. Dalrymple. 1991. Water wave mechanics for engineers and scientists. World Scientific, 353 pp.
Dworak, J. and J. Gomez-Valdes. 2005. Modulation of shallow water tides in an inlet-basin system with a mixed tidal regime. J. Geophys. Res., *110*, doi:10.1029/2003JC001865.
Earwaker, K.L. 1990. Long Island Sound oceanography project : 1988–1990. NOS Oceanographic Circulation Survey Report No. 10, 40 pp with appendices.
Gay, P.S., J. O'Donnell and C. Edwards. 2004. Exchange between Long Island Sound and adjacent waters. J. Geophys. Res., *109*, doi:10.1029/2004JC002319.
Gordon, R. and C. Pilbeam. 1975. Circulation in central Long Island Sound. J. Geophys. Res., *80*, 414–422.
Hench, J. and R. Luettich Jr. 2003. Transient tidal circulation and momentum balances at a shallow inlet. J. Phys. Oceanogr., *33*, 913–932.
Howell, P., J. Benway, C. Giannini, K. McKown, R. Burgess, and J. Hayden. 2005. Long-term population trends in the American lobster (*Homarus americanus*) and their relation to temperature in Long Island Sound. J. Shellfish Res., *24*, 849–857.
Ianniello, J. P. 1977a. Non-linearly induced residual currents in tidally dominated estuaries, PhD thesis, The University of Connecticut, 250 pp.
—— 1977b. Tidally induced residual currents in estuaries of constant breadth and depth. J. Mar. Res., *35*, 755–785.
Inoue, R. and C. Garrett. 2007. Fourier representation of quadratic friction. J. Phys. Oceanogr., *37*, 593–610.
Kaputa, N. P. and C. B. Olsen. 2000. Long Island Sound ambient water quality monitoring program: Summer hypoxia monitoring survey '91–'98 data review. Technical report, Connecticut DEP.
Kenefick, A. M. 1985. Barotropic M_2 tides and tidal currents in Long Island Sound: A numerical model. J. Coastal Res., *1*, 117–128.
Lee, Y. J. and K. Lwiza. 2005. Interannual variability of temperature and salinity in shallow water: Long Island Sound, New York. J. Geophys. Res., *110*, doi:10.1029/2004JC002507.
Li, C. and J. O'Donnell. 1997. Tidally driven residual circulation in shallow estuaries with lateral depth variation. J. Geophys. Res, *102*, 27915–27929.
—— 2005. The effect of channel length on the residual circulation in tidally dominated channels. J. Phys. Oceanogr., *35*, 1826–1840.
Li, C., A. Valle-Levinson, K. Wong, and K. Lwiza. 1998. Separating baroclinic flow from tidally induced flow in estuaries. J. Geophys. Res., *103*, 10405–10418.
Mellor, G. and T. Yamada. 1974. A hierarchy of turbulent closure models for planetary boundary layers. J. Atm. Sci., *31*, 1791–1806.
Murphy, D. L. 1980. A numerical investigation into the physical parameters which determine residual drift in Long Island Sound, PhD thesis, The University of Connecticut, 193 pp.
O'Donnell, J., H. G. Dam, W. F. Bohlen, W. Fitzgerald, P. S. Gay, A. E. Houk, D. C. Cohen, and M. M. Howard-Strobel. 2008. Intermittent ventilation in the hypoxic zone of western Long Island Sound during the summer of 2004. J. Geophys. Res., *113*, doi:10.1029/2007JC004716.

Parker, B. B. 1984. Frictional effects on the tidal dynamics of a shallow estuary, PhD thesis, The Johns Hopkins University, 304 pp.

Parker, C. A. and J. E. O'Reilly. 1991. Oxygen depletion in Long Island Sound: A historical perspective. Estuaries, *14*, 248–264.

Pawlowicz, R., B. Beardsley, and S. Lentz. 2002. Classical tidal harmonic analysis including error estimates in MATLAB using t_tide. Comput. Geosci., *28*, 929–937.

Peters, H. and R. Bokhorst. 2001. Microstructure observations of turbulent mixing in a partially mixed estuary. Part II: Salt flux and stress. J. Phys. Oceanogr., *31*, 1105–1119.

Prandtl, L. 1925. Bericht ueber Untersuchungen zur ausgebileten Turbulenz. ZAMM - Z. Angew. Math. Me., *5*, 136–139.

Prandle, D. 1982. The vertical structure of tidal currents. Geophys. Astro. Fluid, *22*, 29–49.

Proudman, J. 1953. Dynamical Oceanography. Wiley, NY, 409 pp.

Riley, G. A. 1956. Oceanography of Long Island Sound, 1952–1954. Bull. Bingham Oceanographic Collection, *15*, 15–46.

Rippeth, T. P., E. Williams, and J. Simpson. 2002 Reynolds stress and turbulent energy production in a tidal channel. J. Phys. Oceanogr., *32*, 1242–1251.

Schmalz, R. 1993. Numerical decomposition of Eulerian circulation in Long Island Sound, in Estuarine and Coastal Modeling: Proceedings of the 3rd International Conference, M.L. Spaulding, K. Bedford, and A. Blumberg eds., ASCE Press, 294–308.

Signell, R. P., H. J. Knebel, J. H. List and A. S. Farris. 1998. Physical processes affecting the sedimentary environments of Long Island Sound in Estuarine and Coastal Modeling: Proceedings of the 5th International Conference, M. L. Spaulding and A. F. Blumberg, eds., ASCE Press, 400–412.

Souza, A. J. and J. H. Simpson. 1996. The modification of tidal ellipses by stratification in the Rhine ROFI. Cont. Shelf Res., *16*, 997–1007.

Swanson, R. 1976. Tides, in MESA New York Bight Atlas Monograph Series 4, New York Sea Grant Institute, 34 pp.

Valle-Levinson, A., J. Blanco, and M. Frangópulos. 2007. Depth-dependent overtides from internal tide reflection in a glacial fjord. Estuaries Coast., *30*, 127–136.

Valle-Levinson, A. and R. Wilson. 1994. Effects of sill bathymetry, oscillating barotropic forcing and vertical mixing on estuary ocean exchange. J. Geophys. Res., *99*, 5149–5169.

Visser, A. W., A. J. Souza, K. Hessner, and J. H. Simpson. 1994. The influence of water column stratification on tidal profiles in a ROFI system. Oceanol. Acta, *17*, 369–381.

Wilson, R. E., K.-C. Wong, and R. Filadelfo. 1985. Low frequency sea level variability in the vicinity of the East River tidal strait. J. Geophys. Res., *90*, 945–960.

Winant, C. D. 2007. Three-dimensional tidal flow in an elongated, rotating basin. J. Phys. Oceanogr., *37*, 2345–2362.

Wong, K.-C. 1991. The effect of East River on the barotropic motions in Long Island Sound. J. Mar. Res., *49*, 321–337.

Received: *25 March, 2009*; revised: *22 April, 2010*.